Experimental study on droplet size of dispersed oil-water flow

Milad Khatibi

EPT-M-2013-67

MASTER THESIS

For
Stud.techn. Milad Khatibi

Spring 2013

Experimental study on droplet size of dispersed oil-water flow
Måling av dråpestørrelser I olje-vann strøm

Background

The formation of crude oil-water dispersions (emulsions) during oil transportation in pipelines has been a challenge due to the higher effective viscosity of the mixture and the consequent increase of pressure drop. A stable water continuous flow has been found to be a feasible solution of long distance transfer of offshore heavy oil. The droplet size in a dispersed oil-water flow has been found to be one of the key physical parameters that influence the effective (emulsion) viscosity and the stability of water continuous flow.

The direct measurement of droplet size and its distribution in the flow condition has been a challenge for a long time. Most sophisticated measurement techniques for droplet size in oil-water flow are PVM and FBRM. PVM is more accurate than FBRM, but it requires extensive post processing of the data. FBRM can be used as on-line monitor of the droplet size measurement, which is very attractive. Statoil Research Centre at Rotvoll has been using FBRM technique for many years, a lot of data have been acquired. The quality of these valuable data needs to be assessed. This requires the uncertainties of FBRM to be assessed.

Objectives

To quantify the uncertainties of FBRM on the droplet size measurement by PVM technique for dispersed oil-water experiments on the multiphase flow loop at Rotvoll.

The following tasks are to be considered

1. A short literature search on the droplet size measurement of FBRM and PVM techniques for dispersed oil-water flow
2. Laboratory preparation and instrument calibration
3. Pipe flow tests with various crude oil, and various flow conditions, the droplet size will be measured by both FBRM and PVM at the same time.
4. Analysis of the data, and quantify the uncertainties of FBRM measurement for droplet size
5 Suggestions for further work

Within 14 days of receiving the written text on the master thesis, the candidate shall submit a research plan for his project to the department.

When the thesis is evaluated, emphasis is put on processing of the results, and that they are presented in tabular and/or graphic form in a clear manner, and that they are analyzed carefully.
The thesis should be formulated as a research report with summary both in English and Norwegian, conclusion, literature references, table of contents etc. During the preparation of the text, the candidate should make an effort to produce a well-structured and easily readable report. In order to ease the evaluation of the thesis, it is important that the cross-references are correct. In the making of the report, strong emphasis should be placed on both a thorough discussion of the results and an orderly presentation.

The candidate is requested to initiate and keep close contact with his/her academic supervisor(s) throughout the working period. The candidate must follow the rules and regulations of NTNU as well as passive directions given by the Department of Energy and Process Engineering.
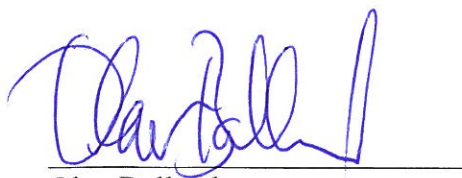
Risk assessment of the candidate's work shall be carried out according to the department's procedures. The risk assessment must be documented and included as part of the final report. Events related to the candidate's work adversely affecting the health, safety or security, must be documented and included as part of the final report.

Pursuant to "Regulations concerning the supplementary provisions to the technology study program/Master of Science" at NTNU §20, the Department reserves the permission to utilize all the results and data for teaching and research purposes as well as in future publications.

The final report is to be submitted digitally in DAIM. An executive summary of the thesis including title, student's name, supervisor's name, year, department name, and NTNU's logo and name, shall be submitted to the department as a separate pdf file. Based on an agreement with the supervisor, the final report and other material and documents may be given to the supervisor in digital format.

☒ Work to be done in lab (Statoil Research Centre)
☐ Field work

Department of Energy and Process Engineering, 16 January 2013

Olav Bolland
Department Head

For Zhilin:

Zhilin Yang, Proff II EPT
Academic Supervisor

Co-supervisors: Bjørnar Hauknes Pettersen, Statoil Research Centre
Ole Jørgen Nydal, EPT

Preface

This study was carried out within the scope of a Statoil project at the Statoil multiphase flow laboratory in Research, development and Innovation (RDI) in Rotvoll-Trondheim office. I gratefully acknowledge the technical and financial support from the flow assurance and multiphase flow department in RDI.

My main word of thank goes to Bjørnar Hauknes Pettersen. I would like to thank him for giving me many detailed instructions on my thesis and helping me to setup the experiment, processing the data and finding solutions to my questions.

I would also like to thank my supervisor at Statoil, Zhilin Yang. He gave me a lot of trust and flexibility when working on the thesis. Without him, I could not have dealt with such a challenging project.

And finally I would like to thank professor Ole Jørgen Nydal and Robert Orr for their helpful advices through experiments and data analysis.

This section would not be complete without thanking my parents who have always supported me during my education.

Abstract

Experimental investigation on droplet sizing measurement techniques both in flow of oil-in-water dispersion and water-in-oil dispersion were performed at the Statoil multiphase flow laboratory in Rotvoll. The focus of these experiments was to analyze the accuracy of chord length distribution (CLD) measured by focus beam reflectance measurement (FBRM technology) in comparison with the droplet size distribution (DSD) measured by a particle video microscope (PVM technology). A beaker – batch test and a flow loop test were employed for a variety of oils spanning over an order of magnitudes in viscosity. The PVM was found to be a useful and accurate measurement device for determining the real droplet sizes and as a calibration method for the FBRM. In the beaker test, The Sauter mean diameter d_{32} was found to be proportional to the maximum (99th percentile) droplet size for both oil-water emulsions and water-oil emulsions. Since the CLD values were underestimating the size in comparison with DSD values, an empirical correlation was developed based on a log-normal distribution to improve the predictive power of the CLD. The dynamic properties of both FBRM and PVM probes were evaluated in beaker tests and flow loop tests. The beaker tests were found to be a reliable and reasonable alternative to flow loop tests. The simplicity of both testing and data collection, combined with the reduced effect of distance between the probes, allow the beaker tests to provide a good estimate of the uncertainty of the FBRM measurement for the water-oil flow in the pipe.

Table of Contents

Abbreviation

BSD	Bubble Size Distribution
CHT	Circular Hough Transformation
CLD	Chord length distribution
DSD	Droplet Size Distribution
d_{32}	Sauter Mean Diameter, $[\mu m]$
d_{43}	Momentum-Volume mean Diameter, $[\mu m]$
d_{99}	99 Percentile of Maximum Diameter Size, $[\mu m]$
d_{max}	Maximum Diameter Size, $[\mu m]$
d_{50}	Median diameter of droplet size distribution, $[\mu m]$
f	Friction factor (fanning)
$f(x)$	Frequency function
FBRM	Focused Beam Reflectance Measurement
HX	Heat Exchanger
L_{50}	Median Length of Chord Length Distribution, $[\mu m]$
PSD	Particle Size Distribution
PVC	PolyVinyl Chloride
PVM	Particle Video Microscope
WC	Water Cut
μ	Diameter Median of Droplet Size Distribution, $[\mu m]$
σ	Standard Deviation of Droplet Size Distribution, $[\mu m]$

1 Introduction

The formation of crude oil-water dispersions (emulsions) during oil transportation in pipelines has been a challenge due to the higher effective viscosity of the mixture and the consequent increase in pressure drop. A stable water continuous flow has been found to be a feasible solution of long distance transport of offshore heavy oil. This is due to the reduced impact of temperature and oil viscosity on the mixture pressure drop. In contrast, when the oil is continuous phase, pressure drop is highly affected by temperature and oil viscosity, since the oil viscosity is changed with temperature. The droplet size in a dispersed oil-water flow has been found to be one of the key physical parameters that influence the effective (emulsion) viscosity and the stability of water continuous flow. (Arirachakaran, Oglesby et al. 1989; Angeli and Hewitt 2000; Lovick and Angeli 2004)

1.1 Project Work

In the specialization project (Khatibi 2012), an experimental investigation of viscous oil-water flow was performed. This experiment was conducted in medium scale flow loop (I.D. = 69 mm, Length ~ 52 m) at the SINTEF Multiphase Flow Laboratory at Tiller. Primol-352 oil and salt water were used in the tests, the oil viscosity ranged from 140-180 cp. The focus of this experiment was on the droplet formation and droplet size development along a horizontal pipe. Oil droplets were generated via a choke downstream the oil-water mixing location. Different choke openings were used to test the droplet formation and evolution process. Two FBRM probes (Lasentec) were installed in the flow line. The experimental data provided the basis for the model development and validation. These models were the maximum droplet size model, the friction model and the log-normal distribution model. It was found that while the FBRM could successfully identify system changes, certain inaccuracies exist in the chord length distributions. For modeling the flow behavior, it needs to have the accurate droplet size information. In this context, the future works were suggested to determinate the uncertainty of FBRM technology. Accurate particle size analysis is a key to study mixing intensity, mixture velocity and the effect of surfactant on viscos oil-in-water emulsion. The basic instrumentation should be proven to work satisfactorily in the parameter range studied. The challenging questions are what is the uncertainty when calculating DSD based on FBRM-CLD measurements? How accurate is it? To answer these questions, an intensive study on FBRM technology under properly defined experiment conditions was needed.

1.2 Aim of the study

The FBRM probe measures the chord length of the droplets CLD, while the PVM probe captures the actual droplets diameter DSD. The aim of this report is to study the uncertainty and limitation of FBRM technology when used to determine the chord length of droplets and provide a proper correlation to convert CLD to DSD. PVM is used as a direct visual method to test the reliability of the FBRM results. Two kinds of test were prepared, beaker – batch tests and flow loop tests. The uncertainty and limitation of PVM technology and image post processing is evaluated in beaker –batch test. The FBRM and PVM probes were employed in the beaker test to study the water-in-oil dispersions and the oil-in-water dispersions for a variety of oils spanning on viscosity. The dynamic behavior for the FBRM and PVM probes were evaluated in beaker tests and flow loop tests for the flow of water-in-oil dispersion. Surfactant was also added to stabilize the water-oil emulsion.

1.3 Background

There are limited experimental literatures in this field of study to find out the uncertainty of FBRM technology. A similar experiment was done on water-oil emulsions, ice and clathrate hydrate formation. In addition, several mathematical techniques exist to translate the CLD into its corresponding PSD.

D. Greaves et al. (2008) found that the FBRM gives undersized droplet distribution in water-oil emulsions. They used PVM to study the uncertainty of CLD measured by FBRM technology in water emulsions, ice and clathrate hydrate formation. While the FBRM can successfully identify changes in ice, hydrate nucleation and growth, certain inaccuracies exist in the CLD. Practically; the FBRM underestimate the droplet size in an emulsion and is unable to measure full agglomerate sizes. He also suggests that any calibration of the FBRM may be highly dependent on physical properties such as refractive index and also dispersion quantity (Greaves, Boxall et al. 2008).

Ruf A. Worlischek and Mazzotti (2000) suggested a mathematical expression for a chord length distribution for spherical particles. A theoretical chord length distribution for each system is generated by importing the measured particles size distribution into equation 1.1:

$$q(s, d_p) = \frac{s}{d_p\sqrt{d_p^2 - s^2}} \; for \; 0 < s < d_p \tag{eq.1.1}$$

Where *s* is a chord length, *dp* is the actual particle diameter, and *q(s, dp)* is the relative probability of obtaining a chord s given the diameter dp (Ruf, Worlitschek et al. 2001).

Bin Hu et al (2005) defined a physical model to originate the probability density function of the CLD for a given DSD, and vice versa. The distribution of the drop size R is described by *P(R)*. The chord length distribution *P(L)*, defined as finding chords of length *L* among all the intersected chords, will be governed by the following issues: Firstly, the size distribution function *P(R)* of drops in the system; Secondly, the conditional probability function $P(L|R)$ of cutting a chord of length L from a drop intersected by the probe with a specific size *R*; Thirdly, the biased sampling probability function $P_B(R)$, which describes the likelihood that a drop of size *R* will be sampled by the probe if a uniform spatial distribution is assumed (Hu, Angeli et al. 2005).

$$P(L) = \int_0^\infty P(L|R)P_B(R)P(R)dR = \int_{L/2}^\infty P(L|R)P_B(R)P(R)dR \tag{eq.1.2}$$

The values of the probability functions $P(L|R), P_B(R)$ depend on the sensor geometry (i.e. needle-tip probe, optical sensor, or laser sheet), the drop shape, and the drop motion. The conditional sampling by FBRM is proportional to r (distance of the closest-approach between the particle center and the probe tip) which leads to:

$$L = \sqrt{D^2 - 4r} \tag{eq.1.3}$$

$$D = 2R \tag{eq.1.4}$$

Mingzhong Li et al. (2006) proposed an effectiveness PSD-CLD model and iterative inversion method which has been validated by experiments. In this model, it is assumed that all particles in a given distribution have the same shape. The model represented as a simple matrix function.

$$C = \frac{N_p}{M_C} AX = AX \qquad\qquad (eq.1.5)$$

Where $A = [A_1 \ ... \ A_j \ ... \ A_M]^T$ is a $M \times N$ matrix and $C = [c_1 \ ... \ c_j \ ... \ c_M]^T$ is the normalized CLD. The matrix A translate the PSD into CLD. N_p is the total number of particles and M_C is the total number of measured chords (Li, Wilkinson et al. 2006).

John A Boxall (2010) has estimated a correlation between PVM and FBRM with an average fitness error of less than 20% given by equation 1.6 and 1.7. The setup was a mixing cell (0.102m internal diameter, 0.229 m height) with a single six-blade impeller (0.051 m diameter) 50.8 mm from the bottom of the cell. The experiment was for the water droplet size in continuous crude oil. The water volume fractions were in a range from 10% to 20% and the oil viscosities were in the range of 1.3 cP-100 cP (Boxall, Koh et al. 2009)

$$PVM\ mean = 0.1481 \times (FBRM\ mean)^2 + 2.9804 \times (FBRM\ mean) \qquad (eq.1.6)$$

$$PVM\ mean = 1.1455 \times (FBRM\ mean)^{1.5469} \qquad (eq.1.7)$$

An average absolute percentage error on polynomial function (eq. 1.6) is 17.2% and on power law function (eq.1.7) is 17.9%. The process of determining the droplet size from the PVM images is done by manually measuring of the droplet diameters.

2   Method

In this chapter, the experimental set-up, measurement techniques, and image processing will be described. In addition, the uncertainty of the PVM probe and the codes in image processing will be evaluated.

2.1   Experimental set-up

The Experiments were performed in two types of arrangement, beaker – batch tests and flow loop tests.

2.1.1   Beaker – Batch tests

The first test was a beaker – batch test, an impeller mixing utility was employed in a wide beaker. The volume of the beaker was 1 liter. PVM and FBRM probes were installed in the beaker at the same level above the impeller blades. This set-up is shown in the figure 2.1. The rotational speed of the impeller was varied from 100 RPM to 2000 RPM. The optical resolution, laser intensity and standard focus position for FBRM and PVM were verified based on procedure described in the manual book.

A white polytetrafluoroethylene reflection cap was employed on the tip of the PVM probe. The PVM was equipped with the optional backscatter laser to increase the view ability. However the cap was useful for the transparent model oils (i.e. Exxsol) to reduce the laser reflection when taking very clear images, it was not useful for the black crude oils (i.e. Troll B, Grane and Peregrino). This is because no movement of the droplets was seen in the images. The use of the PVM probe without cap caused two problems. Firstly, the pictures were dark. Secondly, there were six light dots visible in each droplet and thus the image processing became much more difficult. The rim and the center of the droplets were detected by a Matlab program presented in attachment I. The image processing will be completely described in chapter 2.3. The FBRM probe of each experiment was sampled for a period of 10 minutes. 100-200 images were taken by the PVM probe during the last 5 minutes of the test. The tests were taken at ambient temperature$23℃$.
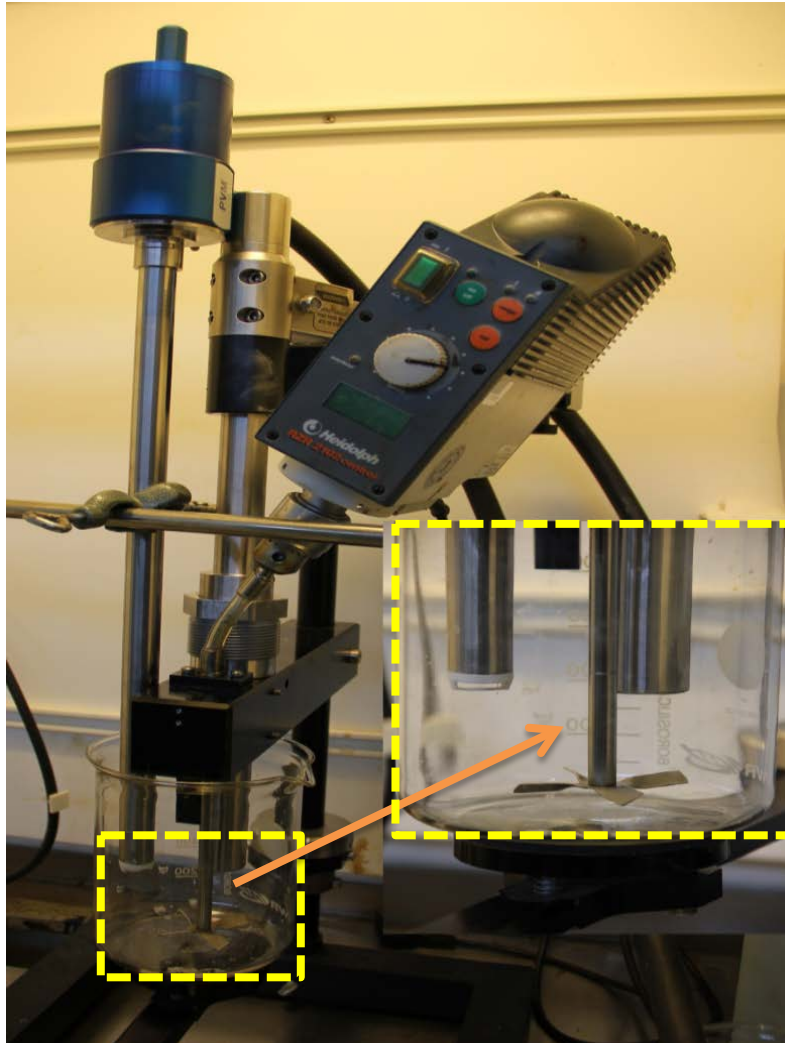
Figure2.1: Beaker - Batch test equipped with FBRM and PVM probes.

2.1.2 Flow Loop Tests

The second experimental arrangement was a closed flow loop. The flow loop with all the equipment is shown in figure 2.2. The major components in the system are two FBRM probes, one located upstream and one located downstream of the flow loop relative to the PVM location, a PVM probe in the middle of stream line, a low shear pump (high pressure displacement pump, Universal II series), a Promass 63M coriolis flowmeter (constraint of 0 - 0,5 Kg/s), a Julabo HC F18 temperature controlled water bath (Maximum temperature 60°C) as a heat exchanger, and horizontal pipe sections with 0.0221 m inner diameter (1 inch) and 0.010 m inner diameter (1/2 inch). A pressure transducer was mounted on each pipe section measuring the pressure drop over a 3m section. The type of heat exchanger was a tube in tube HX. The hot or cold water is circulated around the pipe and moderates the temperature along the pipeline. All piping in the system was made of stainless steel and was insulated. Inner diameter and relative roughness of the pipe in the test section were determined by performing the flow tests of water in the laminar and turbulent flow regimes.

As shown in the figure 2.3, the preferable orientation of the probe is between 30 and 60° to the flow. This directs the flow onto the window surface without creating droplet accumulation. The flow carries droplets close to the window of the best measurement presentation. The pump was controlled by changing the flow rate (0-0.5 Kg/s) by the computer. The useful values (i.e. mass flow water, pressure drop along the pipes, temperatures) were collected for further processing and discussion. The pressure drop and CLD of two FBRM probes in each experimental test were sampled for a period of 15 minutes. Temperature, mass flow rate and pressure drop were measured for every 5 seconds. The 100-200 images were taken by PVM probe in last 5 minutes of the test to ensure that the flow had developed and was in a steady state. Details regarding the droplet size measurements (FBRM and PVM) are given in section 2.2. The tests were taken at ambient temperature23°C.
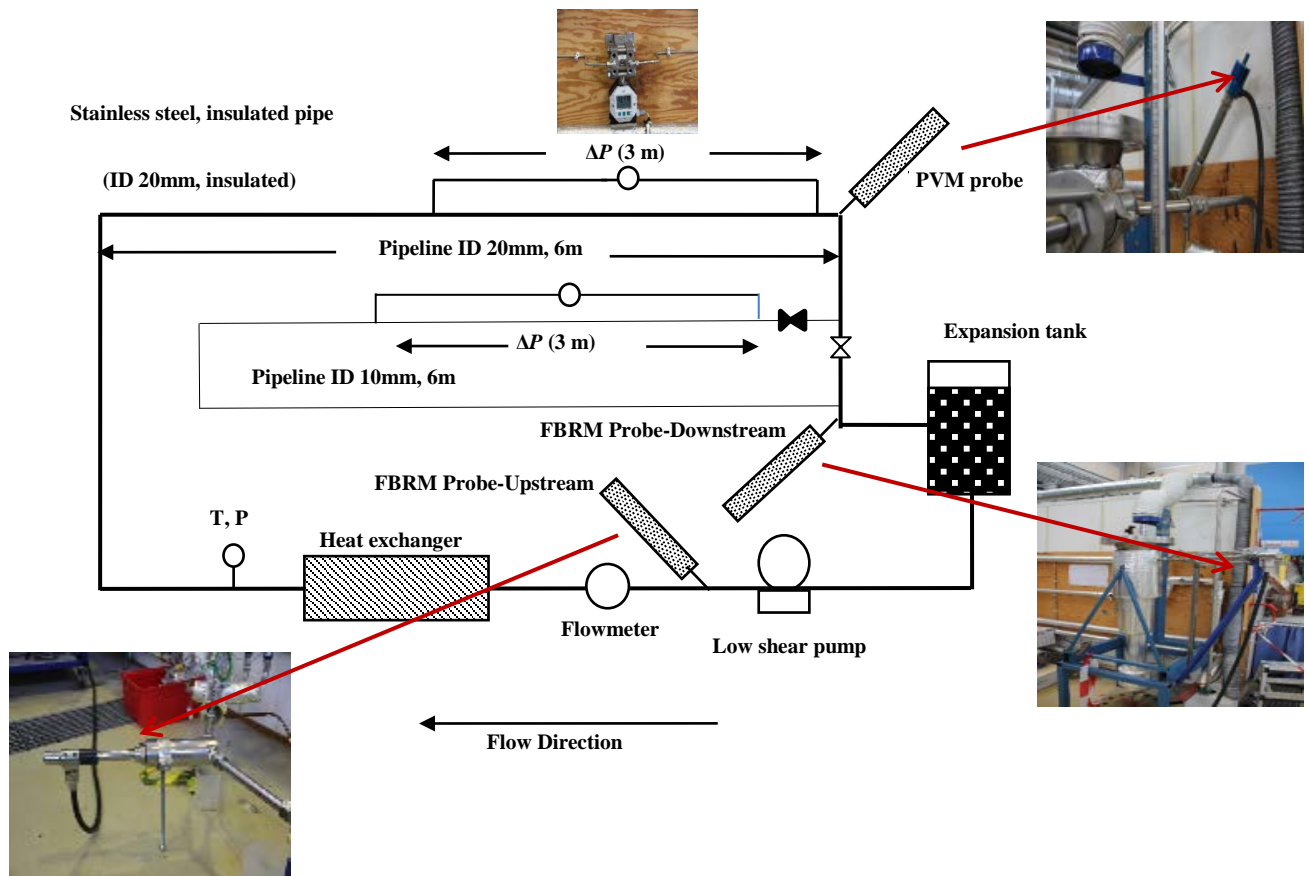
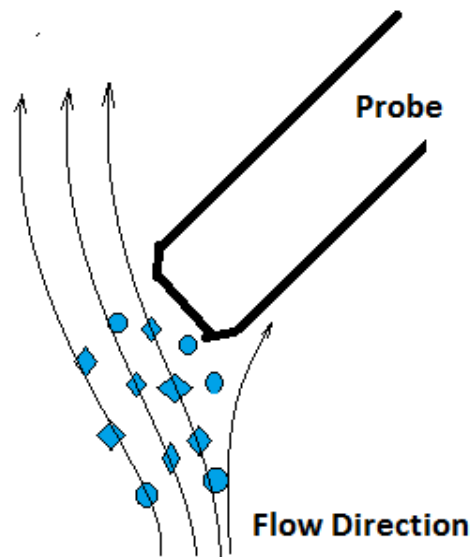Figure2.2: Schematic illustration of the close flow loop system.

Figure 2.3: Position of the probes in the pipe.

2.2 Measurement Techniques

The two main measurement devices, namely the FBRM probe and the PVM probe, will be described in details. These probes can provide in situ droplet characterization at high pressures. It is important to understand how these two measurements work and what procedure they use to measure the droplet size.

2.2.1 Focused Beam Reflection Measurement (FBRM) Probe

The direct measurement of droplet size and its distribution in the flow condition has been a challenge for a long time. Figure 2.4 shows the FBRM Technology (focused beam reflectance measurement). It provides a real time measurement method for changes in droplets dimension and droplets count. On the other hand, it tracks the rate and degree of change in time at full process concentration. The FBRM calculates chord length of the droplets. A chord length (a fundamental measurement of particle dimension) is simply defined as the straight line distance from one edge of a droplet to another edge as shown in figure 2.5. A rotating optical lens at the probe tip deflects the laser. The laser emitted is reflected when it scans across the surface of a particle. Thousands of individual chord lengths are typically measured each second to produce the CLD (O'SULLIVAN, SMITH et al. 2010). The focal point of the FBRM laser can be adjusted into the fluid $(+)$ or inside the probe$(-)$. The focal point position is $-20\mu m$ for the standard FBRM (Group 2004). Heath et al. (2002) discovered the impact of the focal point position on the FBRM measurements, perceiving that changing the focal point more into the fluid increased the number of measured longer chords due to larger particles being less able to approach the measurement window (Heath, Fawell et al. 2002). Turner (2005) recommended that the coarse setting would be more sensitive to agglomerate sizes than primary particle sizes compared to the fine setting, bypassing less detectable edges (Turner 2005).
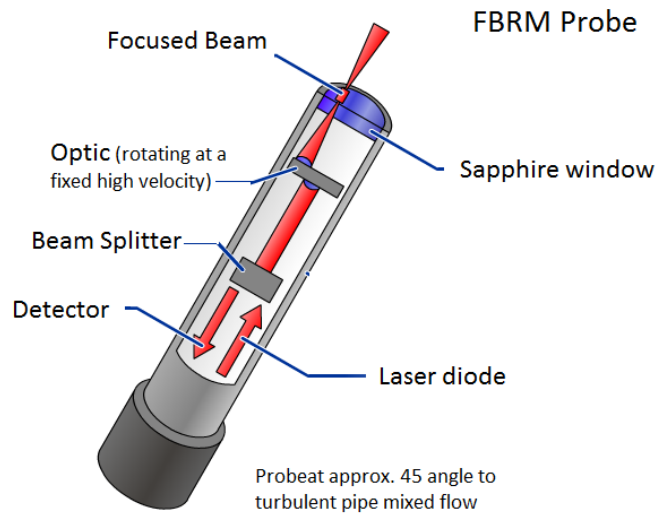
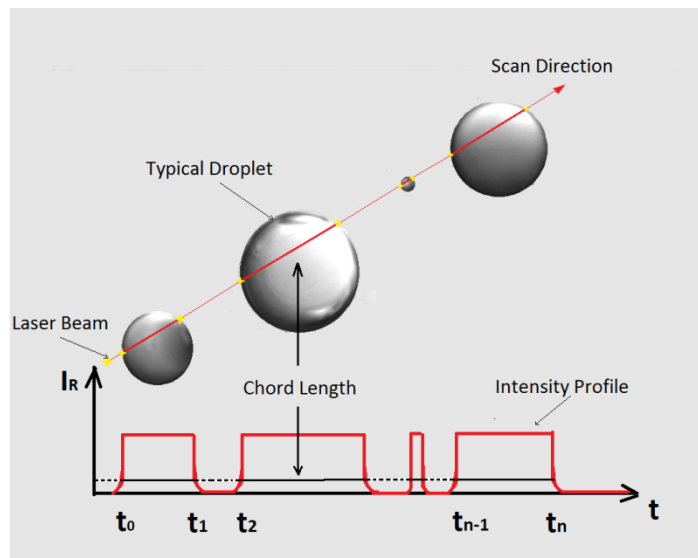Figure2.4: FBRM probe (Tuner, 2005).

Figure2.5: Intensity profile in measuring the chord length of a particle (Tuner, 2005).

2.2.2 Particle Video Microscope (PVM) Probe

PVM Technology is a particle video microscope. It provides in situ digital images and visualizes how particles and droplets are changing as they naturally exist in process. Figure 2.6 shows a PVM probe with high resolution CCD camera and internal illumination source to obtain high quality images even in dark and concentrated suspension or emulsions. The system consists of six independent laser sources arranged circularly in angles of 60° around the objective tube. The probe records digital images of the illuminated lasers with a field view of 1075µm × 850 µm. Figure 2.7 shows how the PVM probe captures images in focus and defocus of the collecting lens. The collecting lens should always be tuned to capture a visible image in detecting the rim of droplets. There is a tunable screw (micrometer adjustment) on top of the CCD camera. This gives us the possibility to tune the collecting lens in focus by looking at the monitor.
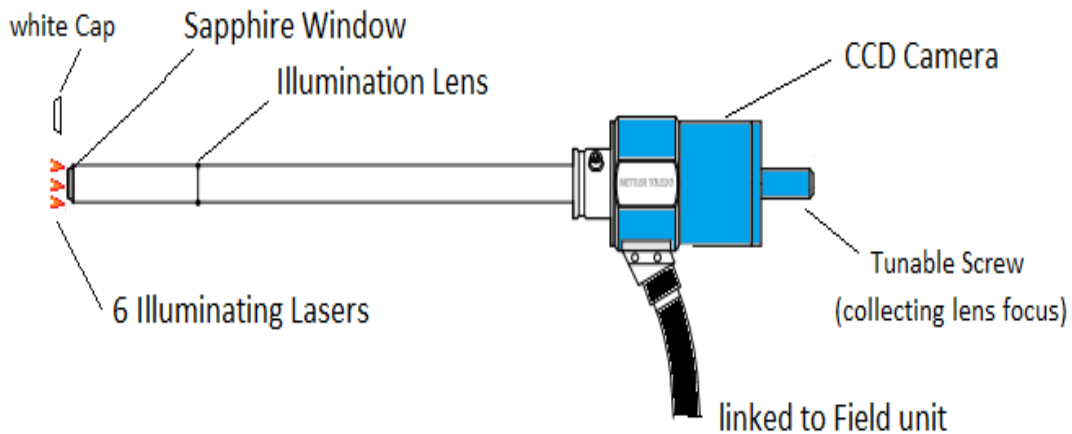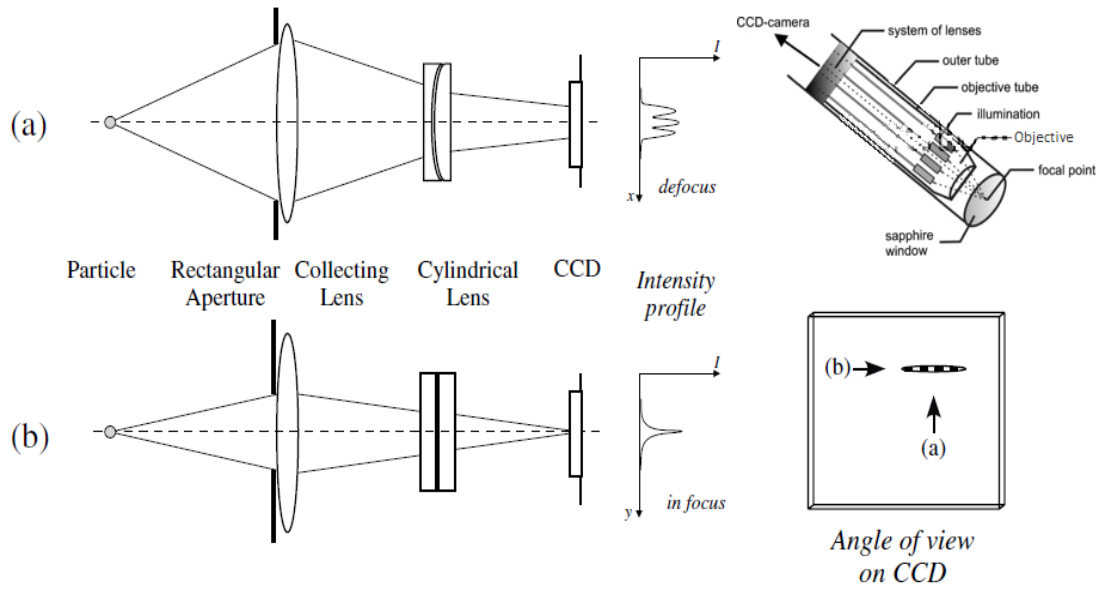

Figure2.6: PVM probe (PVM manual, 2012).

Figure2.7: Illustration of being in focus and defocus of the droplets in PVM probe (PVM manual, 2012).

2.3   Image Processing

Post processing of PVM images was done in Matlab programming software. The main goal of image post processing is to accurately detect the rims of the droplets, measure the diameter of the droplets and give the DSD as an output. It is important to get the accurate approach in the image analysis and understand how Matlab script interprets the images to get the right distribution.

One typical image of oil-water flow is shown in figure 2.8. A big circle together with several small circles inside and around the big one is visible in the image. The horizontal and vertical dimensions of the image are shown based on micro meter and pixel units in table 2.1.

The images were taken by PVM are an 8 bits grayscale image which means that the pixels can have 256 different grayscale values where the value of 0 equals the color black and the value of 255 equals the color white. Figure 2.9 shows sample of these values with focusing in the image.

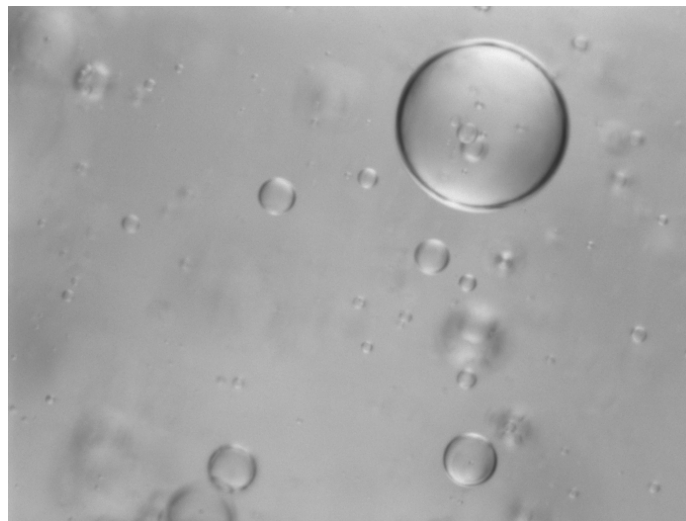Figure2.8: Original image of Exxsol oil-water flow

Table 2.1: Horizontal and Vertical dimensions of the images

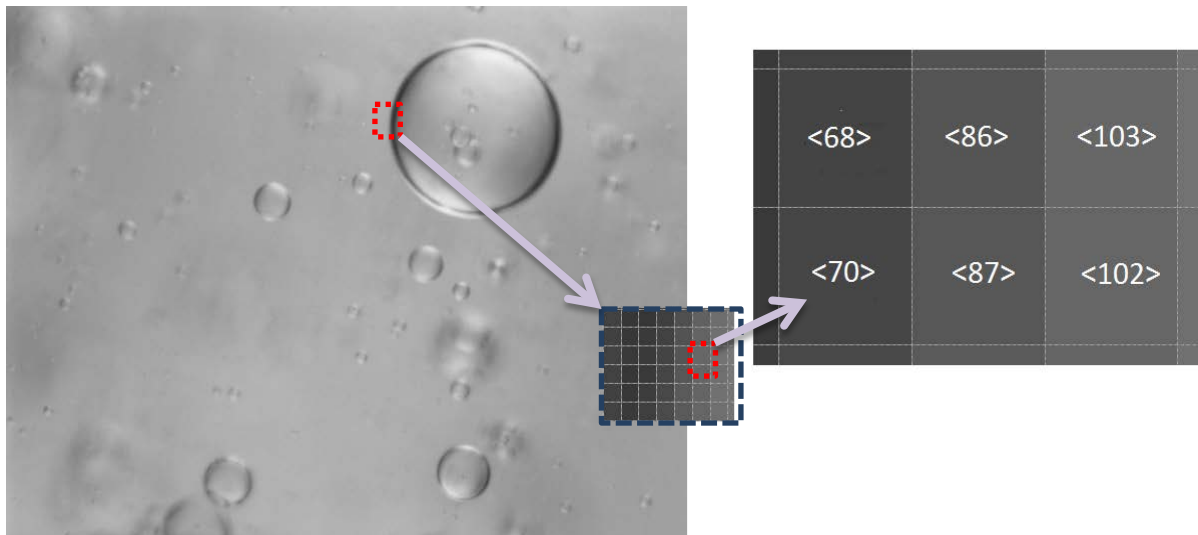| Description	Value
Horizontal dimension of imaging volume	1075 µm
Vertical dimension of imaging volume	850 µm
Number of horizontal CCD pixels	680 Pixels
Number of vertical CCD pixels	512 Pixels

Figure2.9: Magnifier image with pixels grayscale.

As can be seen in the figure 2.9, the pixels of some parts of the droplet rim are very dark compared to the inside or outside of the droplets. The droplet features cannot be related to specific grayscale value because of having bright pixel values in the droplet and the dark pixel values in and out of droplets. So a sophisticated solution is required to detect the droplets. The algorithm used to detect the droplets is described below:

- Image binarisation (adjustment, morphological opening on grayscale, dilating images)
- Edge detection by Circular Hough Transformation, CHT (object polarity, sensitivity and computation method)
- Reverse Circular Hough Transformation, RCHT
- Sum-up and diameter measurement collection
- Histogram anaylsis – DSD output

2.3.1 Image Binarisation

The first step of image binarisation is adjustments of the contrast to enhance and highlight the pixels on the droplets rims in the foreground to remove the pixels that belong to the background. The second step is to perform morphological opening on the grayscale. This is done by measuring the background grayscale and shifting the grayscale to the 0 or 255. For this purpose, the pixels with the grayscale value of less than 75 set to <200-255>, while the pixels with grayscale of more than 75 set to <0>.   The last step is to dilate the detected rims. This means we tried to fill the holes on the rims of droplets and light the rims pixels up. These three steps are represented in the figure 2.10.
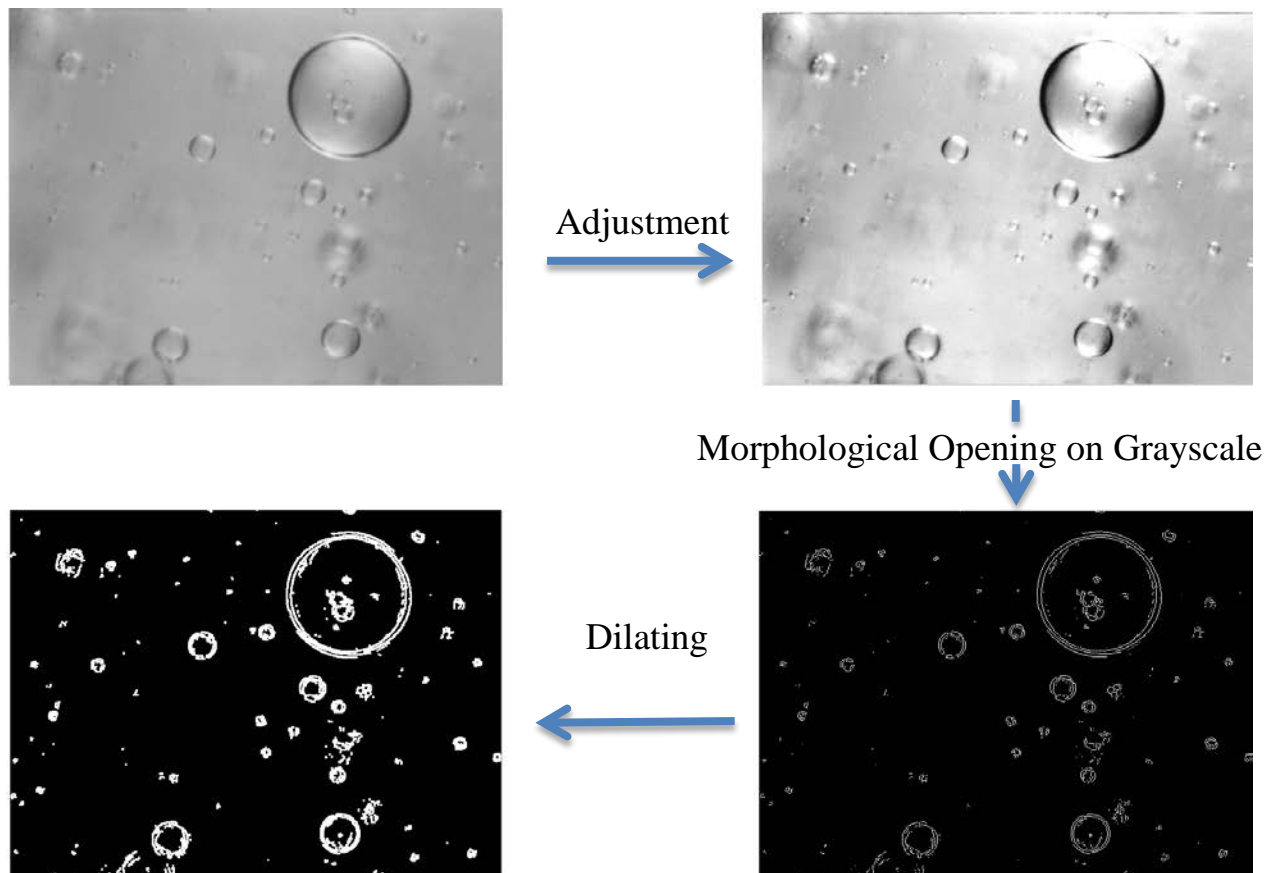
Adjustment

Morphological Opening on Grayscale

Dilating

Figure2.10: Features of steps in image Binarisation

2.3.2 Circular Hough Transformation (CHT)

The circular Hough transformation is defined as an equation for circle that relies on three parameters which are a radius (r) and two dimensions (a and b) representing the coordinate of the circle. The equation of a circle is written as:

$$r^2 = (x - a)^2 + (y - b)^2 \qquad\qquad \text{(eq.2.1)}$$

The parametric variable of the circle is written as equation 2.2:

$$x = a + r \times \cos(\theta)$$

$$y = a + r \times \sin(\theta) \qquad\qquad \text{(eq.2.2)}$$

The CHT is used as a 3D array vector with the two dimensions (representing center coordinate) and the radius (x, y, r). For each edge point, a circle is drawn. The values in the array are increased every time and a circle is drawn with the desired radius over every edge point. The accumulator keep counts of how many circles pass through coordinates of each edge point. The highest count is considered as a diameter of the circles. The coordinates of these highest radius is considered as coordinates center of the circle. Three parameters were considered in this detection. The first one is the object polarity that indicates whether the circular rim is brighter than background. Only circles with the fraction of white pixels larger than 70% (i.e. grayscale value = 178) are accepted. This means only circles that are centered on the brightest spots of the original images are considered for calculation of DSD. The second parameter is a sensitivity factor of the circular Hough transform accumulator array. Higher sensitivity value means higher risk of false detection. The Third one is the computational method of the accumulator array. "Two-Stage" was chosen to compute the CHT accurately. (Baier 2001; Rizon, Haniza et al. 2005).

The reversed Hough transform converts the obtained circles to the image containing circles of radius r. Finally all the diameters are summed up by the for-loop and saved in the excel file for the later calculation of DSD. The histogram distribution analysis according to the DSD range (FBRM: 1-1000 µm) was done in excel sheet. The summary of this procedure for detection of the circles is shown in the figure 2.11. The codes in Matlab software are described in the attachment I.
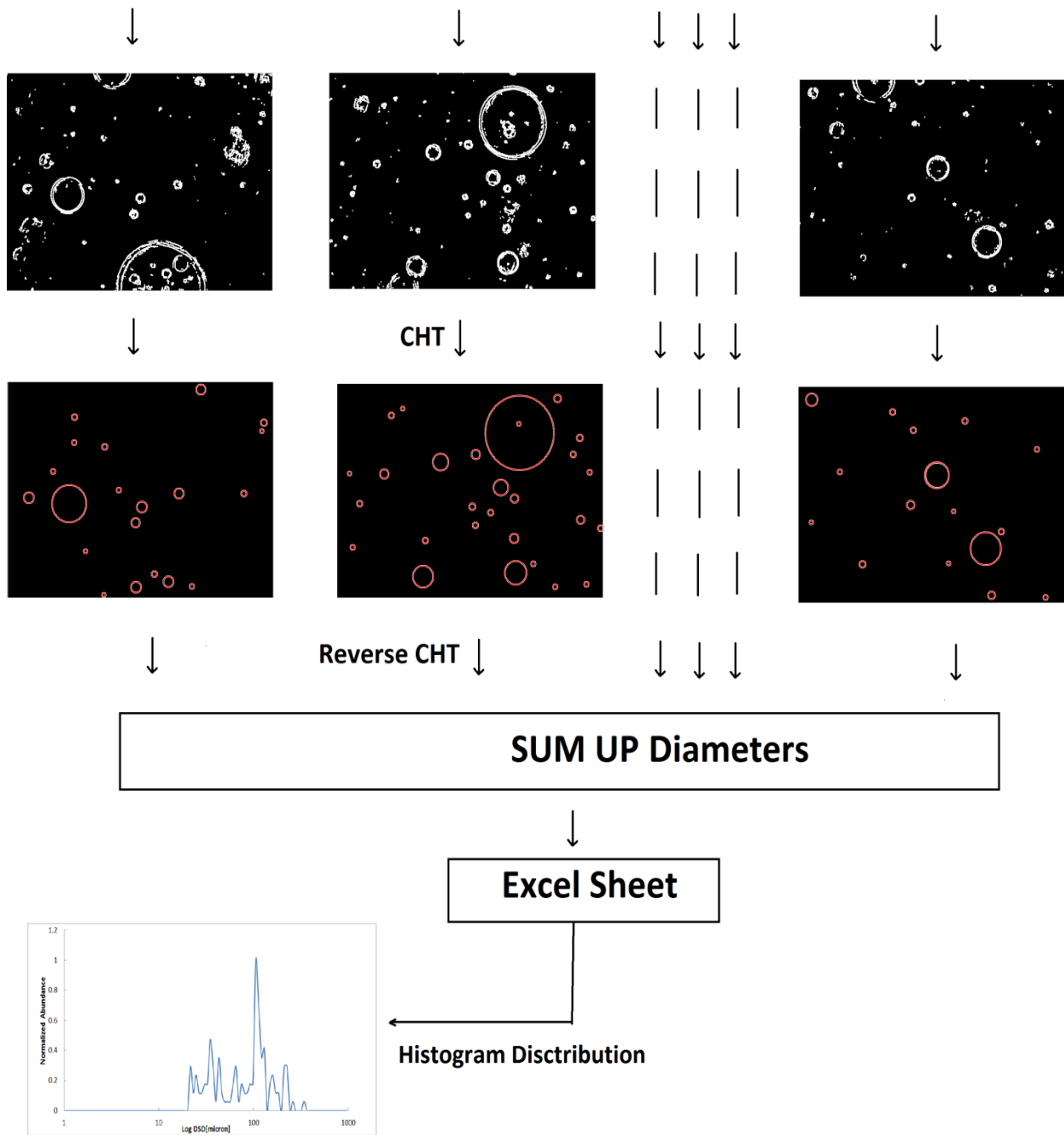
Figure2.11: CHT and RCHT of image processing, diameter collection, and Histogram analysis.

2.4   Uncertainty assessment of image post processing

The main issue of post processing is to check the uncertainty and limitation of the Matlab script in detecting the droplets. To find out how accurate this post processing is, several samples were chosen. These images were opened and measured manually in IC-FBRM software and then the results were compared with Matlab results. The IC-FBRM is a software for controlling the FBRM probes, monitoring and collecting the raw data in an excel file.

The comparison between DSD from Matlab analysis and DSD from manual calculation is done for different oils to verify the Matlab calculation. The size of population in counting the droplets is one of the key in calculating the uncertainty. The size of population for Matlab Analysis is around 1000 and the size of population for Manual distribution is around 800. The higher the number of counting, the more precise the DSD will be. Figure 2.12 represents the trends of Matlab and manual calculation of DSD with parametric studies of d_{32} and d_{99} for Exxsol, Troll B and Grane oils. As can be seen in the figure, the trend of d_{32} and d_{99} shows the accuracy of Matlab analysis very well. 0% to 7% uncertainty is found and is mostly due to the unclear images captured from the crude oils.
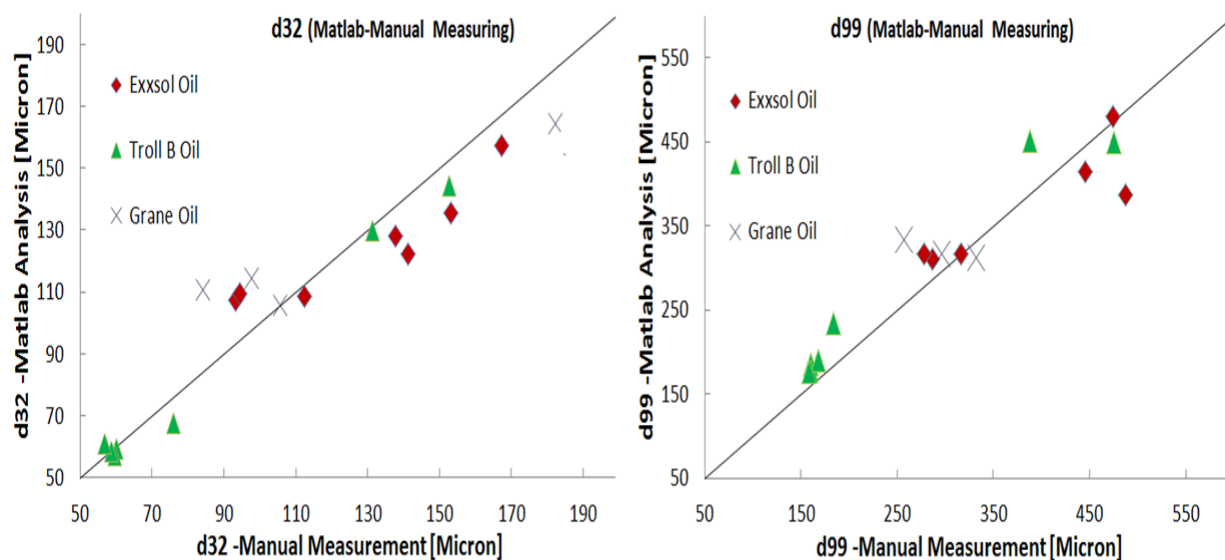

Figure 2.12: Comparison of the d_{32} (in the left graph), and d_{99} (in the right graph) calculated from Matlab analysis with d_{32}, and d_{99} calculated from manual measurement in IC-FBRM software for Exxsol, Troll B and Grane oils at different WC (10% -90%)

2.5 Uncertainty assessment of FBRM and PVM in polyvinyl chloride reference system

The polyvinyl chloride (PVC) suspended at 8.33% mass fraction in water phase was provided as a calibration reference sample. The reference particle size distribution (Reference PSD) was also prepared from Lasentec/Mettler Toledo. The beaker test was employed with the mixing velocity of 400 rpm. The raw data measured with FBRM and PVM probes were used to evaluate the uncertainty of the chord length distribution (CLD) and the particle size distribution (PSD) in comparison with the Reference PSD in the PVC system. The PVM images were analyzed with the PVM software. The shapes of particles were not round and could not be detected with the Matlab script, so the blob algorithm in the PVM software, made by the Mettler Toledo Company, was utilized for detecting the particles in the PVC system. In addition, the normalized volume distribution is utilized for comparison the CLD, the PSD and the Reference PSD in figure 2.13. As can be seen in normalized distribution, both the CLD and the PSD profiles are closely matched to the Reference PSD profile, while in the cumulative distribution, the PSD is matched better to the reference PSD for the big particles. Table 2.2 represents the parametric studies of d_{32}, d_{43}, and d_{99} for CLD, PSD, and Reference PSD. The maximum diameter d_{99} in CLD is larger than d_{99} in Reference PSD, while it is almost the same for PSD and the Reference PSD ($d99 = 397 \mu m$). In contrast, the d_{32} is larger for the PSD than the CLD in comparison with the d_{32} in the Reference PSD. The figure 2.14 is a normalized abundance for the CLD and the Reference PSD. As can be seen, very small particles ($1 \mu m < $ Cord Length $ < 10 \mu m$) are detected by FBRM that gives an uncertainty in the particle sizing.

Comparison the CLD and the PSD with the Reference PSD in beaker test
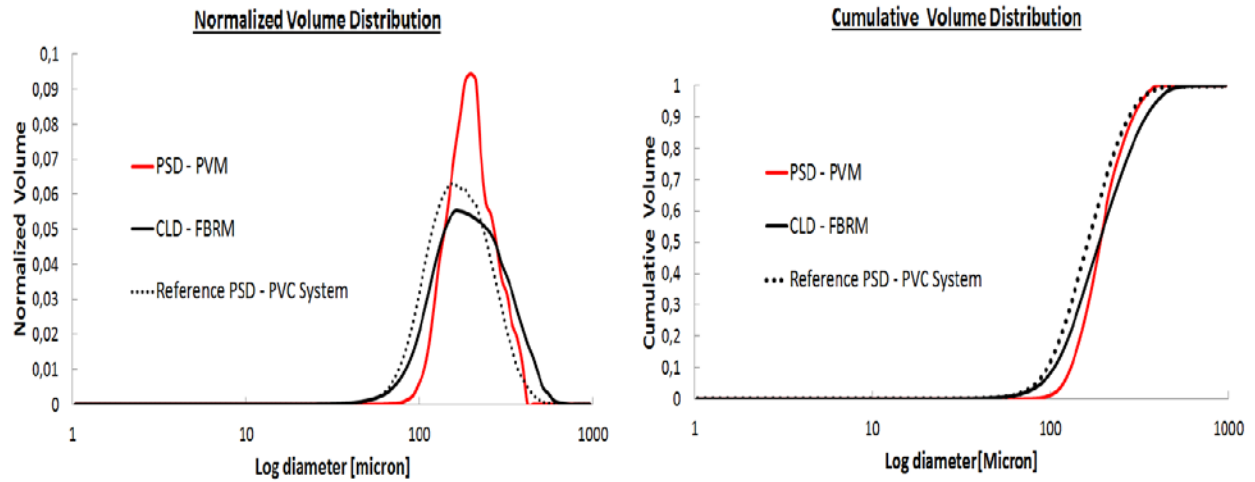
Figure 2.13: Normalized volume and cumulative volume of the CLD measured with the FBRM probe, the PSD measured with the PVM probe, and the Reference PSD from PVC system.

Table 2.2: Main parametric studies d_{32}, d_{43}, and d_{99} on the Reference PSD from the PVC system, the CLD measured with the FBRM probe and the PSD measured with the PVM probe.

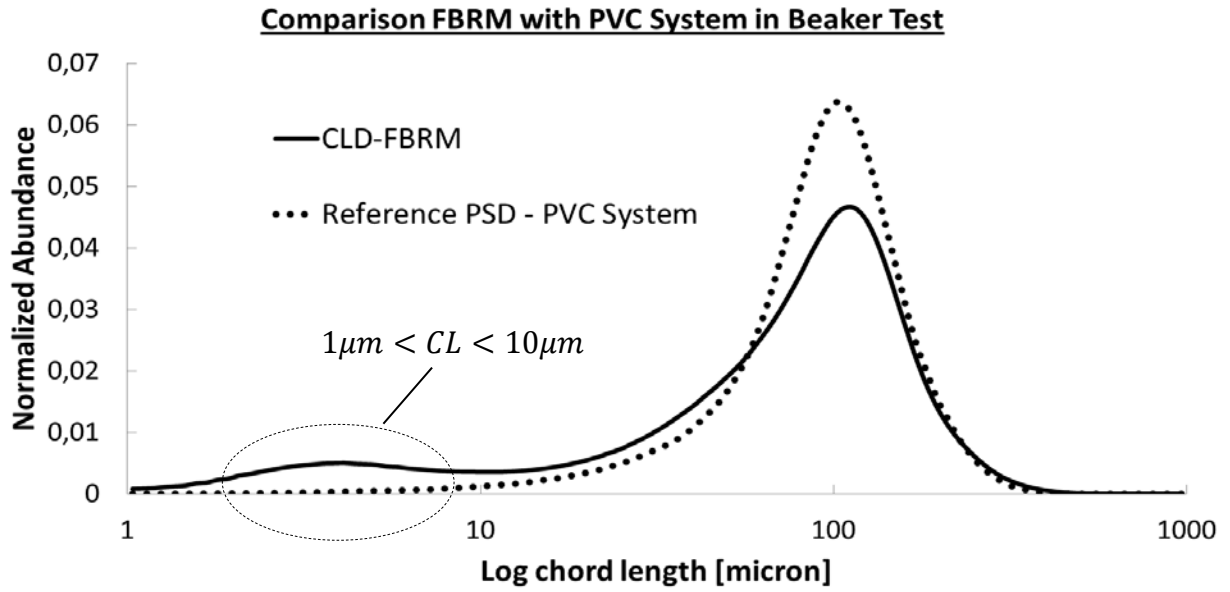| Distributions	d_{32}	d_{43}	d_{99}
Reference PSD – PVC System	153	182	397
CLD – FBRM probe	175	214	484
PSD – PVM probe	189	207	371

Figure 2.14: Normalized Abundance of the CLD measured with the FBRM probe and the Reference PSD from the PVC system.

3 Experiments (Test Matrix)

In this chapter the fluid properties used in the experiments, test matrix, and variable parameters changed in beaker – batch test and flow loop test are described.

3.1 Fluid parameters

The liquids in this study were Exxsol oil, Troll B oil, Grane oil, Pregrino oil and water (3.5% NaCl). Table 3.1 shows the material information of these oils. Some tests were tried to be done with Pregrino oil for this study. Due to the high stickiness of this oil, it stuck on the lenses of both the FBRM and the PVM probes and reduced the accuracy of measurement. At high water cut (more than 60 %), the viscosity and the stickiness of the oil increased rapidly and converted to tar. the fluids in the beaker distinct to separate tar and water. This also caused the tar stuck to the glass, the rod and the blades of the impeller, and then the impeller started to rotate the beaker. So the test stopped. The experiment continued with Grane oil which also has a high viscosity but it is not sticky.

Table 3.1: Fluid properties at atmospheric pressure and temperature

Fluids	Density (tabulated) [kg/m³]	Dynamic Viscosity [cP] (@23°C)	Kinematic Viscosity [mm²/s] (@23°C)	Shear rate [S⁻¹] (@23°C)
Water + 3.5% NaCl	~1023	1	1	-
Exxsol D60	786	1.3	1.65	1047
Exxsol + 0.1% Span 80	786	1.3	1.65	1045
Troll B	895	24.5	27.5	355
Grane	934	245	262	47.8
Pregrino	925 (@50°C)	391.5 (@50°C)	423	27.3

3.2 Test Matrix

The parameters that were varied in beaker - batch test are:

- Oil
- Surfactant
- Mixture velocity
- Water cut (volume of water divided to the total volume)

A summary of the set parameters for beaker test are shown in table 3.2.

Table 3.2: Overview of the experimental set-parameters used in beaker – batch test. Column 1: mixer, column 2: various oils, column 3: nominal mixture velocity, column 4: nominal water cut.

Mixer	Oils	U_{mix} [RPM]	WC [%]
Impeller	Exxsol	1500	10, 30, 40, 50, 60, 70, 90
Impeller	Troll B	1500	10, 30, 40, 50, 60, 70, 90
Impeller	Grane	1500	10, 30, 40, 50, 60, 70, 90
Impeller	Pregrino	1500	10,30,40,50,60
Impeller	Exxsol	400, 700 , 1000, 1300, 1500, 1700, 2000	10, 20
Impeller	Exxsol + 0.1% Span 80	400, 700 , 1000, 1300, 1500, 1700, 2000	10, 20

The parameters that were varied in flow loop test are:

- Surfactant (with and without Span 80)
- Mass flow rate [kg/s]

A summary of the set parameters for flow loop test are shown in table 3.3.

Table 3.3: Overview of the experimental set-parameters used in flow loop test. Column 1: mixer, column 2: Exxsol with and without surfactant, column 3: nominal mass flow rate, column 4: nominal water cut.

Mixer	Oils	Mass Flow rate [Kg/s]	U_{mix} [m/s]	WC
Shear Pump	Exxsol	0.064, 0.136, 0.196, 0.247, 0.0297, 0.326	0.16, 0.33, 0.47, 0.59, 0.70, 0.77	10%
Shear Pump	Exxsol + 0.05% Span 80	0.075, 0.138, 0.192	0.18, 0.33, 0.46	10%
Shear Pump	Exxsol + 0.1% Span 80	0.080, 0.141, 0.194	0.19, 0.34, 0.47	10%

4   Results and Discussion

In this chapter, the results of both beaker test and flow loop test are used to study the uncertainty of CLD measured by FBRM probe. Normalized volume distributions and cumulative distributions are used to develop proper correlations to convert the CLD to the DSD for water-in-oil dispersion and oil-in-water dispersion flow. The surfactant was added at water cut 10% to study the dynamic change of CLD and DSD at different velocities. In addition, the flow loop test and the beaker test are compared in the last chapter.

4.1   Beaker Test

In the beaker test, the CLD and DSD at Water cut 10% - 30% are chosen to study the uncertainty of FBRM on water-in-oil dispersion flow and water cut 70% - 90% are chosen to study the uncertainty of FBRM on oil-in-water dispersion flow. All the calculations were done based on volume distribution. The important parameters of droplet distribution such as square weighted diameter d_{32}, and d_{99} (99 percentile size of droplet distribution) are calculated to develop the distribution models and correlations. The d_{99} from CLD and d_{99} from DSD are estimated as maximum droplet size.

4.1.1   Water-in-Oil Dispersions

In this part of the study, the uncertainty of CLD using FBRM probe in water-in-oil dispersion is evaluated. The experimental data of the beaker test at water cut 10% and 30% are chosen. The CLD and DSD of the water-in-oil dispersion are shown for Exxol oil and Troll B oil in figure 4.1 and 4.2. In the left pictures the normalized volume distribution of droplets are shown. The CLD profile is flatten for both oils; this means the FBRM probe measures a wide range of droplet size. In contrast, the DSD profile is narrow with higher abundance; this means the PVM probe measures the accurate droplet size in limited range which can be supported by images in attachment II. In the right pictures the cumulative distribution of both CLD and DSD are shown. The chord length cumulative distribution extends well beyond the size of the droplets. In addition, the FBRM probe detected small droplets less than 50 micron which were not captured in the PVM images; however, the droplet size distribution is vastly undersized by the FBRM probe.

The difference of d_{32} and the difference of d_{99} in CLD and DSD are calculated as equation 4.1.

$$d_{32-Difference} = \frac{d_{32-DSD} - d_{32-CLD}}{d_{32-DSD}}$$

$$d_{99-Difference} = \frac{d_{99\,volume\,-DSD} - d_{99\,volume-CLD}}{d_{99\,volume-DSD}} \qquad \text{(eq. 4.1)}$$

The table 4.1 shows the average of differences in d_{32} and d_{99} between CLD and DSD. The difference in d_{99} is higher for Troll B oil than the Exxsol oil, while the Troll B oil has the lower differences in d_{32} than the Exxsol oil. The reason of this behavior could be due to be different type of oils. The Troll B is a kind of black crude oil and more viscos than Exxsol oil, while Exxsol oil is a transparent model oil. For the cases with Grane oil, The PVM images were not captured clearly because the droplets were not clear at low water cut due to darkness and high viscosity of Grane oil, hence it was not possible to draw the distributions for this oil.

Table 4.1: Average of differences in d_{32} and d_{99} between CLD and DSD for water-in-oil dispersions

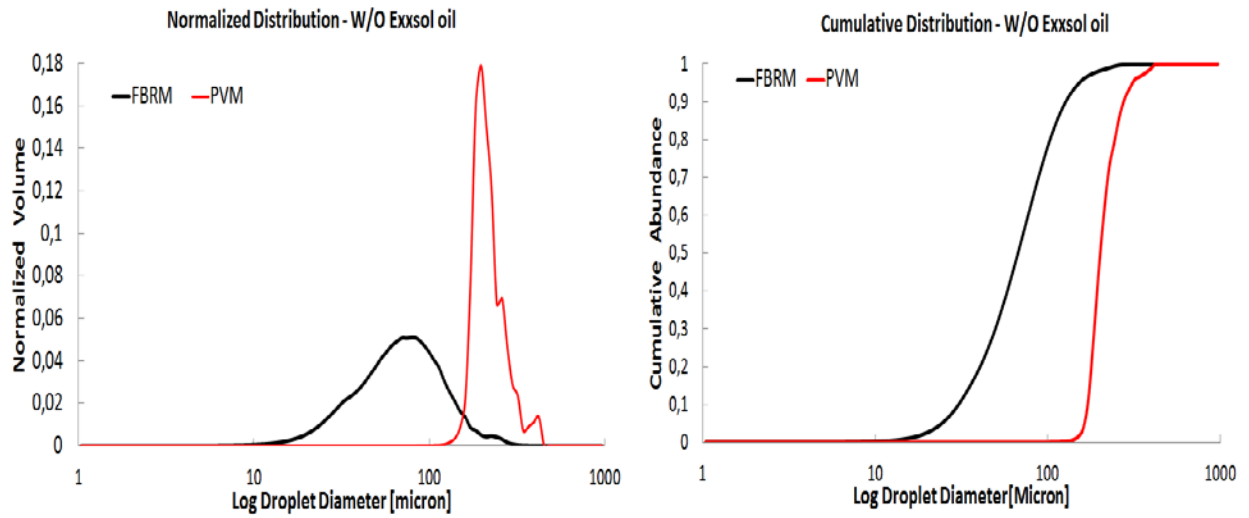| Oil	Speed	WC	$d_{32\text{-CLD}}$	$d_{32\text{-DSD}}$	$d_{99volume\text{-CLD}}$	$d_{99volume\text{-DSD}}$	Average $d_{32\text{-Difference}}$	Average $d_{99\,-Difference}$
-	RPM	%	μm	μm	μm	μm	%	%
Exxsol	1500	30	63	213	227	401	**70**	**43**
Troll B	1500	30	33	103	151	320	**68**	**53**

Figure 4.1: The normalized distribution and cumulative distribution of CLD and DSD in water-in-oil dispersion for Exxsol oil at WC=30%
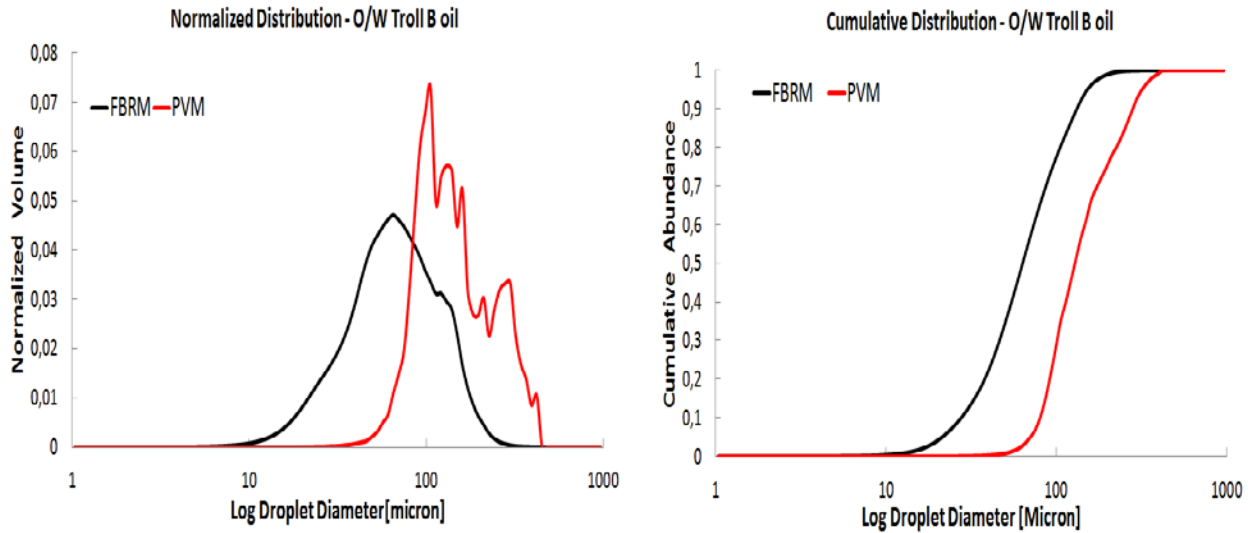

Figure 4.2: The normalized distribution and cumulative distribution of CLD and DSD in water-in-oil dispersion for Troll B oil WC=30%

The droplet size distribution could be well described by a log-normal distribution. For this purpose all cases with WC = 10% - 30% are chosen. Normalized volume CLD and DSD, d_{mean} and d_{99} of each case of experiment are used to investigate a possible conversion from CLD to DSD. The value of normalized volume in CLD and DSD are considered as y and Y, and the value of chord length in CLD and droplet diameter in DSD are considered as x and X as shown in figure 4.3. Regarding to the normalized distribution, the area under the normalized curve of both CLD and DSD are equal to one. If we divide the x axis of the curve according the arithmetic mean μ and standard deviationσ, the area under the CLD curve could be related to the area under the DSD curve. If we divide the interval into n subintervals of equal width,Δx and from each interval choose a point, x_i then the definite integral of $f(x)$ from μ-3σ to μ+3σ is written as equation4.2

$$\lim_{n\to\infty} \sum_{1}^{n} f(x).\Delta x = \int_{\mu-3\sigma}^{\mu+3\sigma} f_{CLD}(x).d_x = \int_{\mu-3\sigma}^{\mu+3\sigma} f_{DSD}(x).d_x$$

(eq.4.2)

Where $f(x)$ is a function of the frequency of droplet size distribution.

The general form of log-normal distribution function $f(x)$ is expressed as equation 4.4 (Packer and Rees 1972):

$$f(x) = \frac{1}{x\sigma\sqrt{2\pi}} \exp[\frac{(\ln x - \mu)^{\wedge}2}{2\sigma^2}]$$

(eq.4.4)

Where μ and σ are diameter median and standard deviation of the distribution.
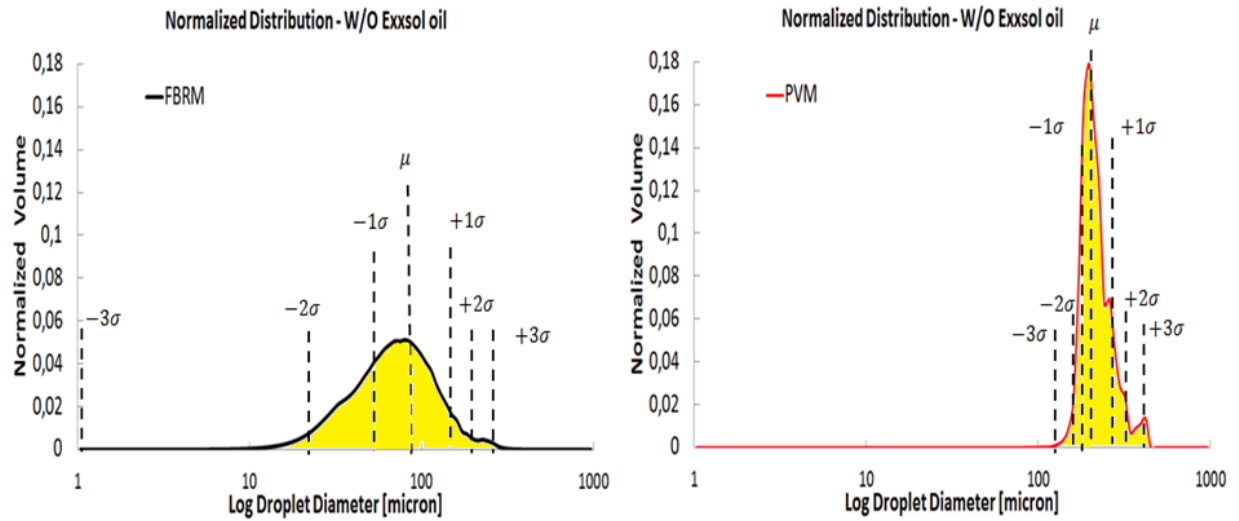
Figure 4.3: Normalized CLD and DSD of Exxsol at water cut 30%.

The Sauter mean diameter d_{32} of DSD agreed very well with the mean droplet diameter (μ) for the best fit log normal distribution. An average absolute percentage error between the two means is 2.3%. Based on normal droplet size distribution model, the arithmetic mean μ and standard deviation σ can be calculated with equation 4.5. These equations are closely matched to the experimental data of CLD and DSD.

$$\mu_{CLD} = \ln d_{32-CLD} \quad , \quad \mu_{DSD} = \ln d_{32-DSD}$$

$$\sigma_{CLD} = \sqrt{2 * (\ln d_{43-CLD} - \ln d_{32-CLD})}$$

$$\sigma_{DSD} = \sqrt{2 * (\ln d_{43-DSD} - \ln d_{32-DSD})} \tag{eq.4.5}$$

Where Sauter mean diameter d_{32} and moment–volume mean diameter d_{43} are defined as equation 4.6:

$$d_{32} = \frac{\sum_1^n N_i \times d^3}{\sum_1^n N_i \times d^2}$$

$$d_{43} = \frac{\sum_1^n N_i \times d^4}{\sum_1^n N_i \times d^3} \tag{eq.4.6}$$

Where N_i is the abundance of the droplets size.

The correlations for d_{32} and d_{43} with d_{99} in DSD are calculated in equation 4.7 and shown in figure 4.4. The d_{99} is considered as maximum droplet diameter.

$$d_{32} = 0,43 * d_{99}$$

$$d_{43} = 0,47 * d_{99}$$

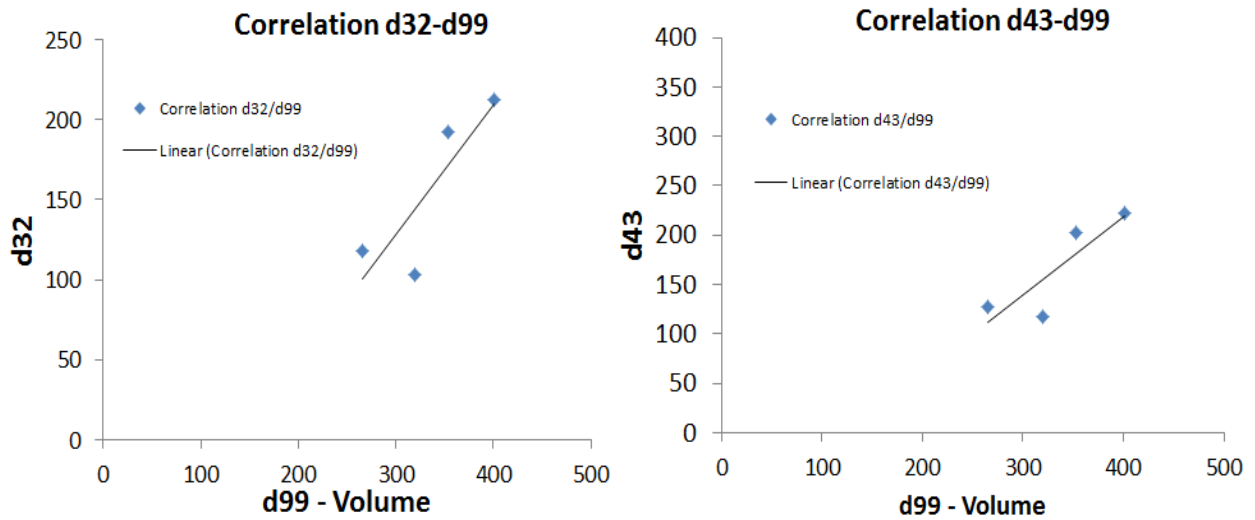<div style="text-align: right">(eq.4.7)</div>

Figure 4.4: The correlation between d_{32} with d_{99} based on volume distribution in the left picture and the correlation between d_{43} with d_{99} based on volume distribution in the right picture.

The convert CLD-DSD model is developed as shown in equation 4.8. The conversion of CLD to DSD for Exxsol oil and Troll B oil at WC=30% are calculated based on n = 40 subinterval in integral and shown in figure 4.5. The conversion will be more accurate by increasing subintervals. The converted DSD is closely matched to the experimental DSD that confirms the robustness of these correlations.

$$
\begin{cases}
1 \leq x \leq \mu - 2\sigma & \rightarrow \acute{\mu} - 3\acute{\sigma} \leq X \leq \acute{\mu} - 2\acute{\sigma} \quad, & Y_1 = 0, \ (Y_1 + Y_2) = \frac{(y_1 + y_2)(x_2 - x_1)}{(X_2 - X_1)} \\[3ex]
\mu - 2\sigma < x \leq \mu - 1.8\sigma & \rightarrow \acute{\mu} - 2\acute{\sigma} < X \leq \acute{\mu} - 1.8\acute{\sigma} \quad, & (Y_{\acute{\mu}-2\acute{\sigma}} + Y_{\acute{\mu}-1.8\acute{\sigma}}) = \frac{(y_{\mu-2\sigma} + y_{\mu-1.8\sigma})(x_{\mu-2\sigma} - x_{\mu-1.8\sigma})}{(X_{\acute{\mu}-2\acute{\sigma}} - X_{\acute{\mu}-1.8\acute{\sigma}})} \\[3ex]
\ldots \\[2ex]
\mu < x \leq \mu + 0.2\sigma & \rightarrow \acute{\mu} < X \leq \acute{\mu} + 0.2\acute{\sigma} \quad, & (Y_{\acute{\mu}-2\acute{\sigma}} + Y_{\acute{\mu}-1.8\acute{\sigma}}) = \frac{(y_{\mu} + y_{\mu+0.2\sigma})(x_{\mu} - x_{\mu+0.2})}{(X_{\acute{\mu}} - X_{\acute{\mu}+0.2})} \\[3ex]
\ldots \\[2ex]
\mu + 2.8\sigma < x \leq \mu + 3\sigma \approx d_{99} & \rightarrow \acute{\mu} + 2.8\acute{\sigma} < X \leq \acute{\mu} + 3\acute{\sigma} \approx \acute{d}_{99} \quad, \quad \ldots
\end{cases} \qquad \text{(eq.4.8)}
$$

Conversion of CLD to DSD - W/O Exxsol oil

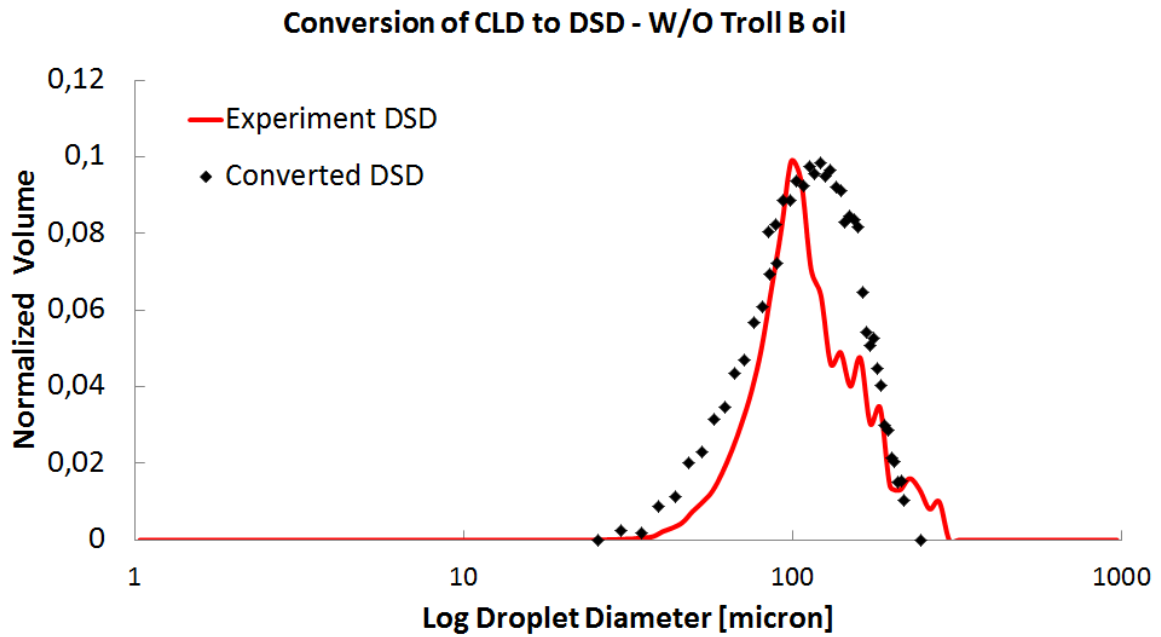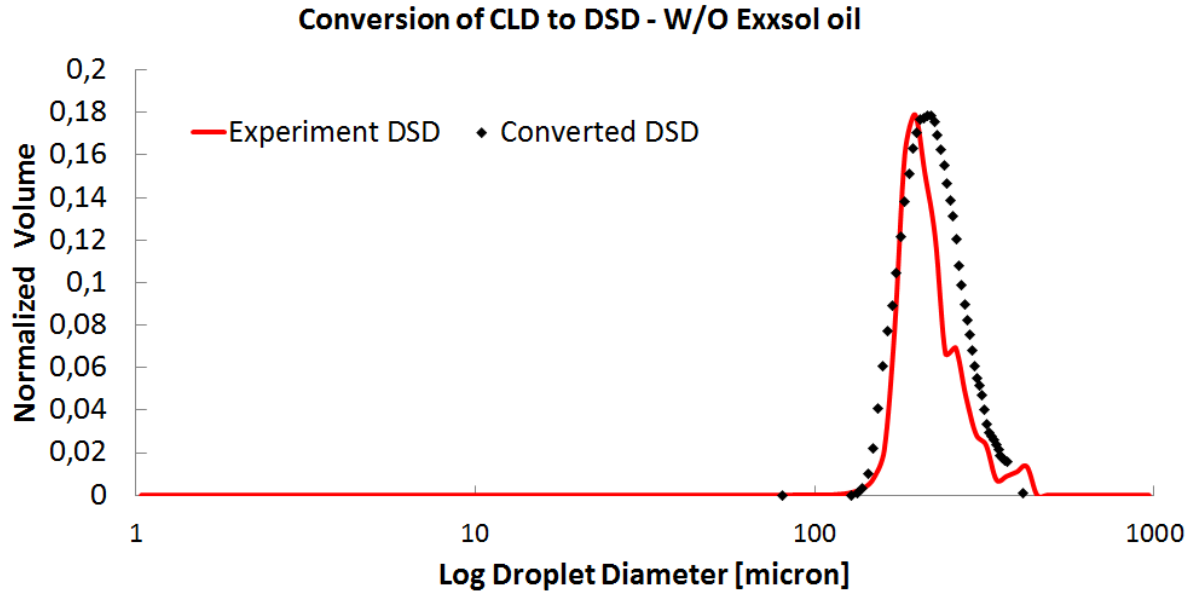**Conversion of CLD to DSD - W/O Troll B oil**

Figure 4.5: The experimental DSD and Converted DSD for Exxsol oil and Troll B oil in flow of water-in-oil dispersion (WC=30%).

4.1.2 Oil-in-Water Dispersions

In this part of the study, the uncertainty of CLD using FBRM probe in oil-in-water dispersion is evaluated. The experiment data of beaker test at water cut 70% and 90% are chosen. The CLD and DSD of the oil-in-water dispersion are shown for Exxol oil, Troll B oil and Grane oil in figure 4.6, 4.7 and 4.8. In the left pictures the normalized volume distribution of droplets are shown. It is also clear here that the FBRM probe detects small droplets less than 50 micron which they were not captured in the PVM images, while the droplet size distribution is undersized by the FBRM technology. The difference of d_{32} and the difference of d_{99} in CLD and DSD are also calculated based on equation 4.1. The table 4.2 shows the average of differences in d_{32} and d_{99} between CLD and DSD of the oils. The average of differences in d_{99} is lower for the Exxsol oil (43%) and higher for the Grane oil (59%), while the differences in d_{32} is almost the same for these oils. The reason could be because of different types of oil. Troll B is a black crude oil and more viscos than Exxsol oil, However, Grane oil is much more viscos than Troll B. Exxsol is a transparent model oil. For the Grane oil, The PVM images were captured very clearly because the oil droplets are big and have very clear rims in water phase.

Table 4.2: Average of differences in d_{32} and d_{99} between CLD and DSD for oil-in-water dispersions

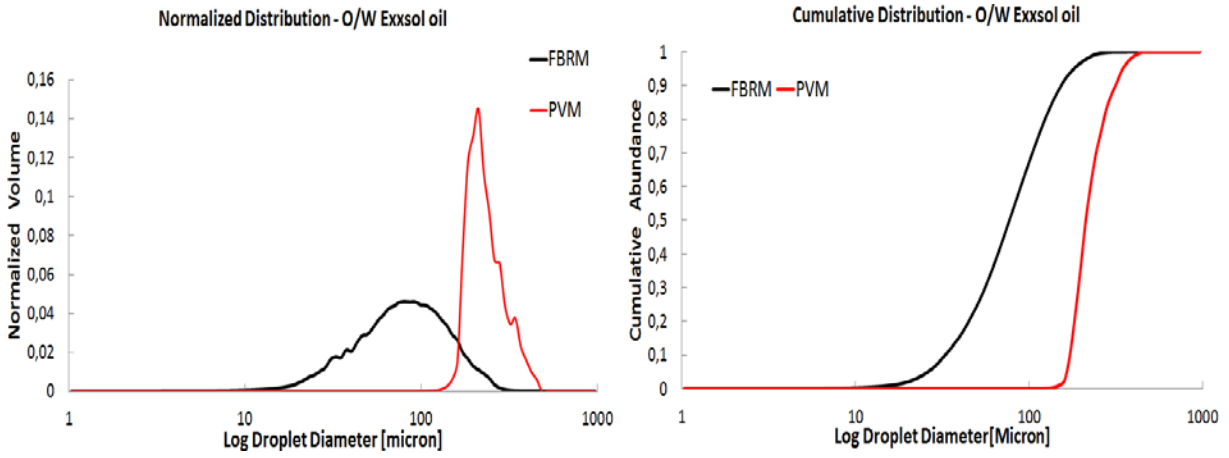| Oil	Speed	WC	$d_{32\text{-CLD}}$	$d_{32\text{-DSD}}$	$d_{99\text{volume-CLD}}$	$d_{99\text{volume-DSD}}$	Average $d_{32\text{-Difference}}$	Average $d_{99\text{-Difference}}$
-	RPM	%	μm	μm	μm	μm	%	%
Exxsol	1500	70	68	225	235	411	**70**	**43**
Troll B	1500	70	36	128	202	394	**72**	**49**
Grane	1500	70	66	215	175	400	**69**	**56**

Figure 4.6: The normalized distribution and cumulative distribution of CLD and DSD in oil-in-water dispersion for Exxsol WC=70%
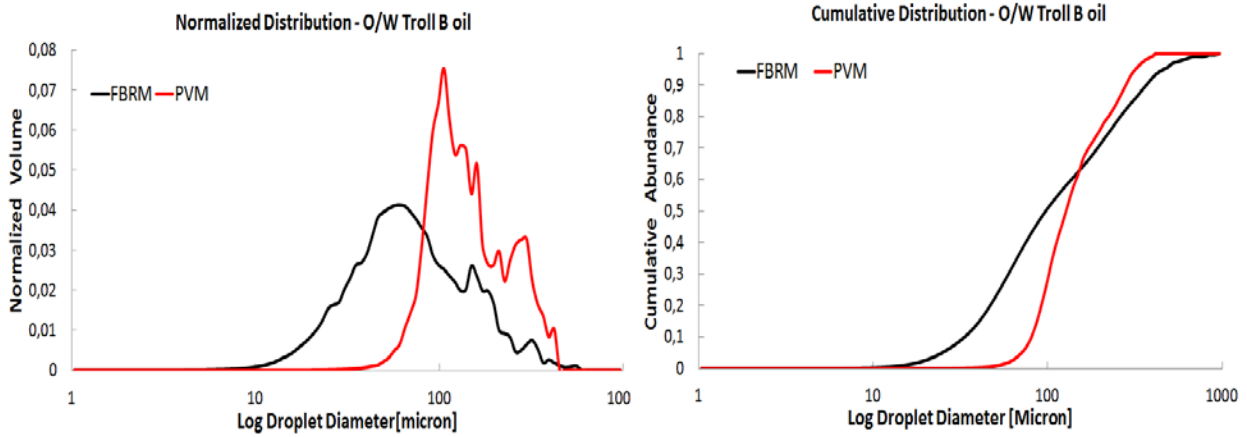

Figure 4.7: The normalized distribution and cumulative distribution of CLD and DSD in oil-in-water dispersion for Troll B WC=70%
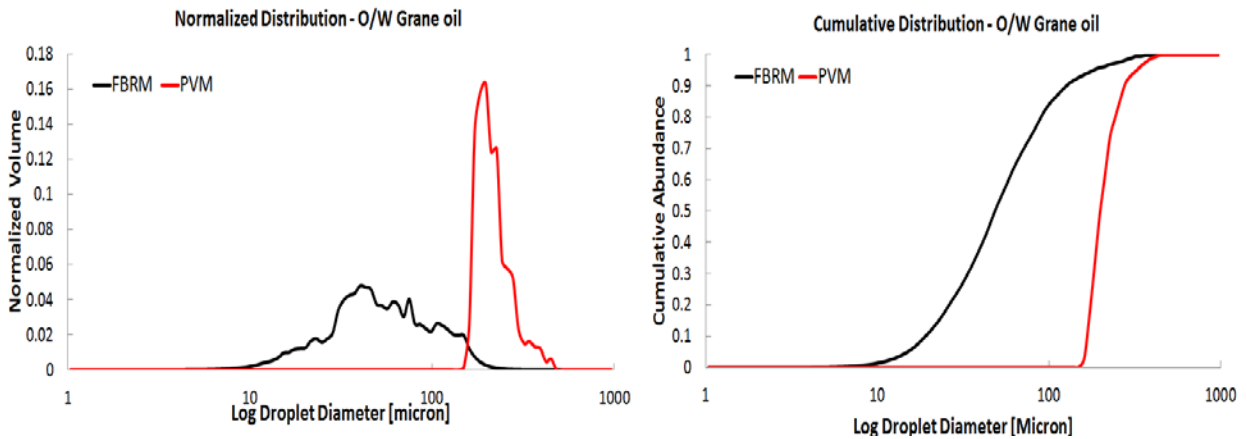

Figure 4.8: The normalized distribution and cumulative distribution of CLD and DSD in oil-in-water dispersion for Grane WC=70%

The correlations are made for d_{32} and d_{43} with d_{99} and shown in equation 4.10. The d_{99} is considered as maximum droplet diameter.

$$d_{32} = 0{,}51 * d_{99-volume}$$

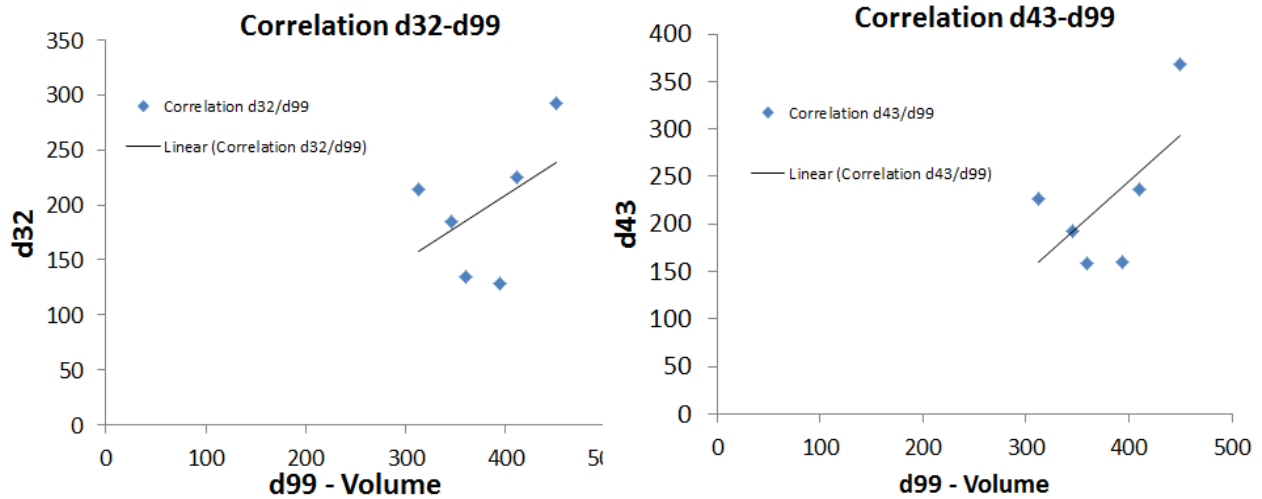$$d_{43} = 0{,}58 * d_{99-volume} \hspace{4cm} \text{(eq.4.10)}$$

Figure 4.9: The correlation between d_{32} with d_{99} based on volume distribution in the left picture and the correlation between d_{43} with d_{99} based on volume distribution in the right picture.

The conversion CLD-DSD model developed in equation 4.9 is utilized for Exxsol, Troll B and Grane oil at water cut 70%. The conversion of CLD to DSD are calculated based on n = 40 subinterval in integral and shown in figure 4.10. The conversion will be more accurate by increasing the subinterval of integral. The converted DSD is closely matched to the experiment DSD that confirms the robustness of these correlations.
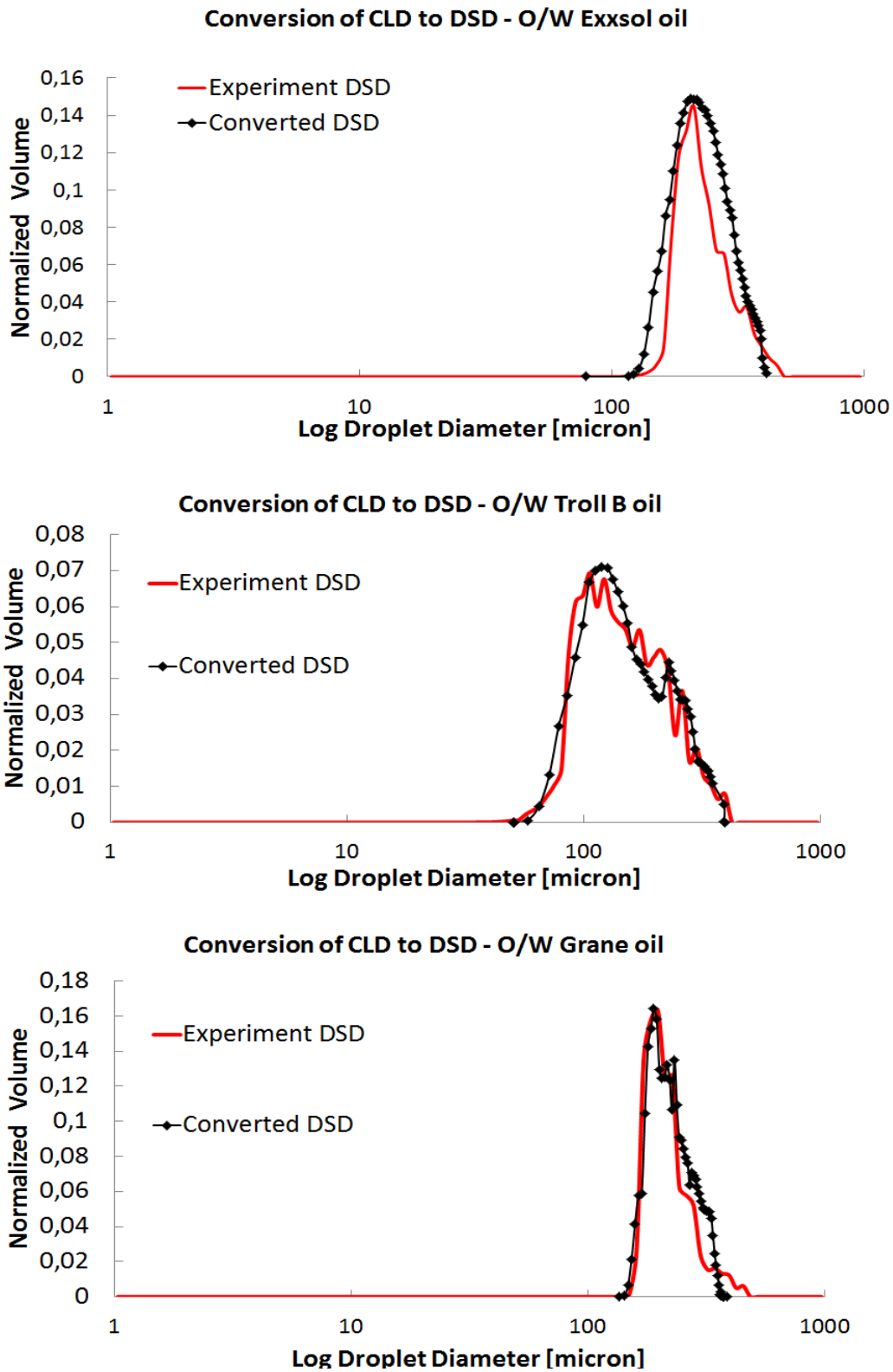
Figure 4.10: The experiment DSD and Converted DSD for Exxsol, Troll B, and Grane oil in the flow of oil-in-water dispersion (WC=70%).

4.1.3 Stabilized water-in-oil dispersion

In this study, the influence of dynamic properties of FBRM probe and PVM probe in water-in-oil dispersion is evaluated. The experimental data of beaker tests for Exxsol oil at water cut 10% with 0.1wt% surfactant is chosen. The water cut of 10% was used for the measurements as it was determined to give suitable PVM images without being too sparse at high droplet sizes or too dense with small droplets. The surfactant was added to increase the possibility to reach the very small droplets (less than $10\mu m$) and have the homogeneous mixture. The rotational speed was changed from 400 rpm to 2000 rpm to have dynamic changes in distributions. The CLD and DSD of the test are shown in figure 4.12. The effect of rotational speed during the time evolution of median of chord lengths L_{50} and median of droplet diameters d_{50} are shown in figure 4.11. The median decreases in both CLD and DSD when the rotational speed increases. In the left picture on FBRM measurement, the L_{50} is reached to the equilibrium value around 5 microns in 1300 rpm and continued until 2000 rpm. In contrast, in the right picture on PVM measurement the d_{50} is reached to the equilibrium value of 8 microns in 1700 rpm. This means the PVM shows the dynamic evolution in widely range of speed compare to the FBRM.
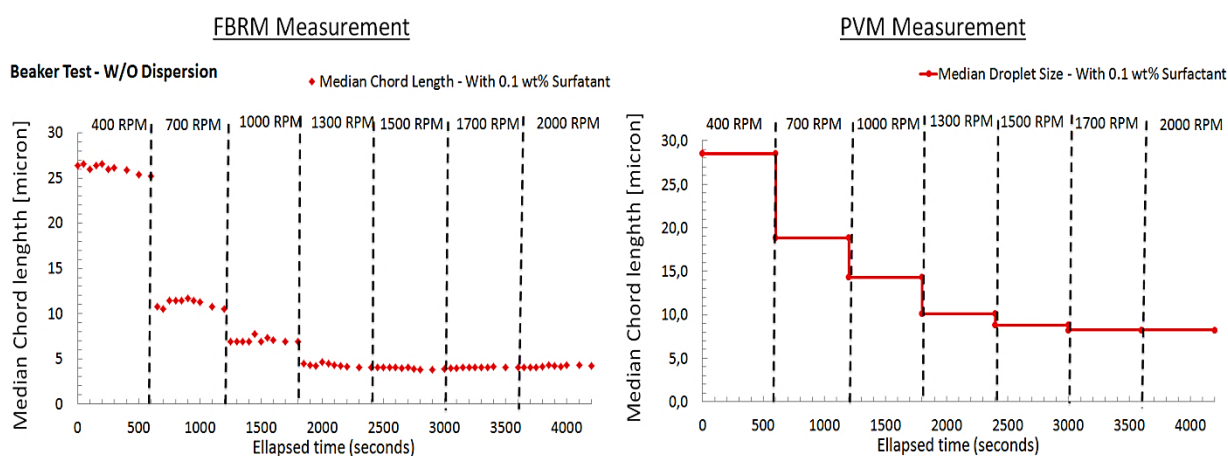

Figure 4.11: Effect of rotational speed during time evolution of L_{50} and d_{50}.

Obvious differences can be found in normalized distribution and cumulative distribution in figure 4.12. In terms of data analysis, the evolution of chord length distribution and droplet size distribution can be seen in both normalized distribution and cumulative distribution with increase in rotational speed. The profiles in both CLD and DSD move to the smaller droplets with increase in rotational speed. This is due to breaking of big droplets to the smaller droplets by increasing the rotational speed of the impeller. The clear issue can be seen in these pictures at

high rotational speed is that the normalized count rate of chord length decreases slightly in CLD profiles with increase in rotational speed, while the normalized count rate of droplets in DSD profiles rises and is almost constant at high rotational speed.
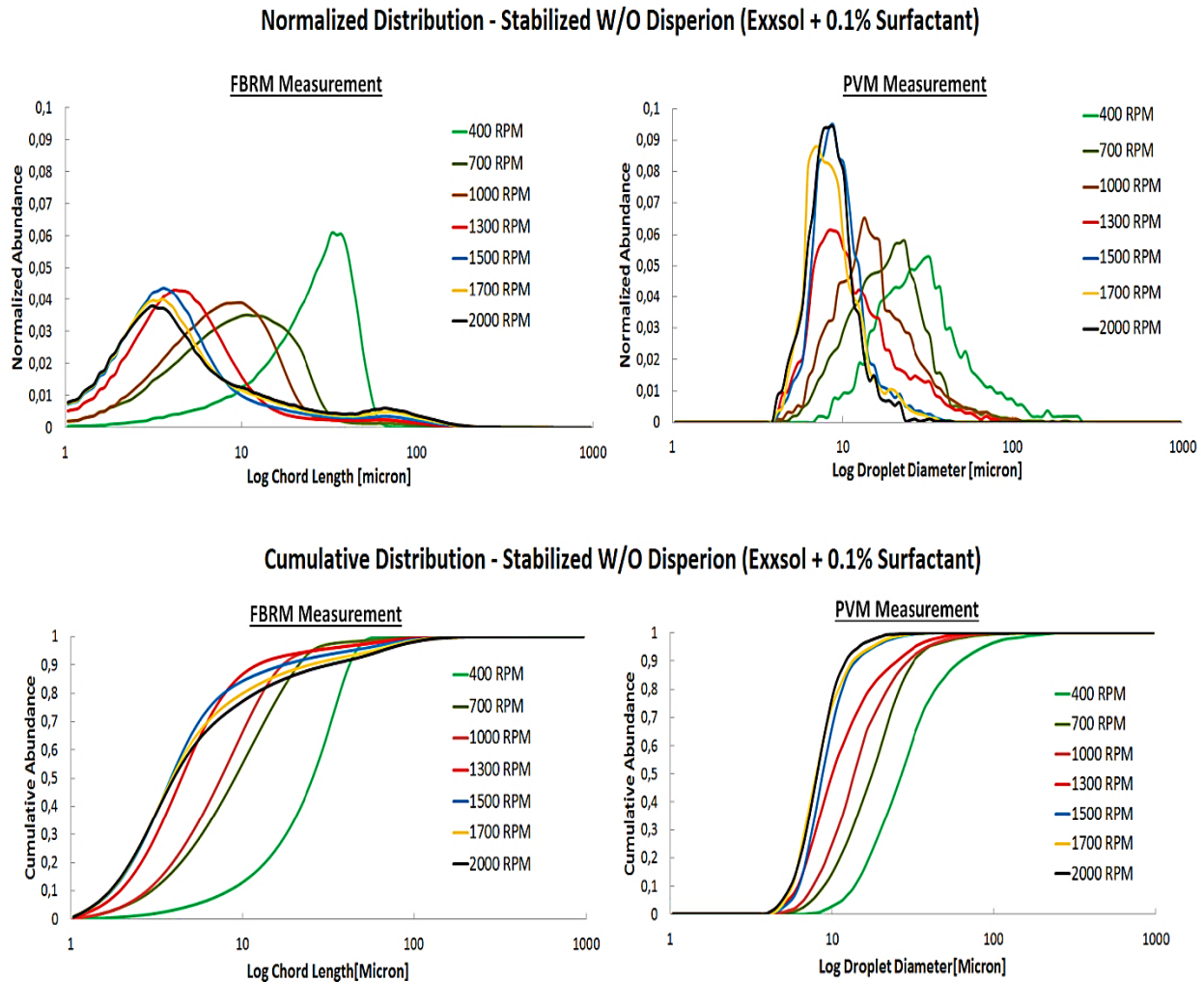

Figure 4.12: Effect of change in rotational speed on normalized distribution and cumulative distribution of CLD using FBRM measurement in the left pictures and DSD using PVM measurement in the right pictures.

4.2 Flow loop tests

The closed flow loop was employed to study the dynamic properties of FBRM and PVM for the flow in the pipe in comparison with Beaker test. The flow loop consists of two FBRM probes in upstream and downstream regarding to the PVM probe. The PVM probe was located in the middle of the stream. Firstly, The Exxsol oil with water cut 10% was used to study the flow of unstable water-in-oil dispersion. Secondly, the surfactant was added to this flow to study the flow of stabilized water-in-oil dispersion. Meanwhile, the uncertainty of FBRM measurement for this study is evaluated.

4.2.1 Flow of unstable water-in-oil dispersion

The mixture velocity was changed from 0.16 m/s to 0.77 m/s to have a dynamic change in CLD and DSD. Figure 4.13 shows the count number of chord length by the FBRM probes positioned upstream and downstream. The chord lengths were divided into four groups. For the upstream FBRM, the number of chord length less than 50 microns increases by an increase in velocity due to break up of droplets after the pump, while the number of chord length more than 50 micron decreases. The flow developed along the pipeline and was measured by the downstream FBRM probe. The number of chord length less than 50 microns is almost constant until velocity 0.59 m/s and rapidly increases 0.6% in velocity 0.77m/s, while the number of chord length between 50 and 150 microns is gradually raised until 0.33 m/s and rapidly jumped to 0.15% in velocity 0.59 m/s. In contrast, the number of chord length between 150 and 300 microns increases until velocity 0.59 m/s and decreases to almost 0% in 0.77m/s. In addition, Figure 4.14 shows the dynamic change of DSD with increase in velocity of the flow. Regarding to the location of PVM probe in the middle of the stream, the effect of distance between PVM probe and FBRM probes should be reduced. This is done by adding surfactant to stabilize the water-in-oil dispersion. In the next chapter it is tried to analyze the fully developed flow as an approach of evaluating the accuracy of FBRM probe.
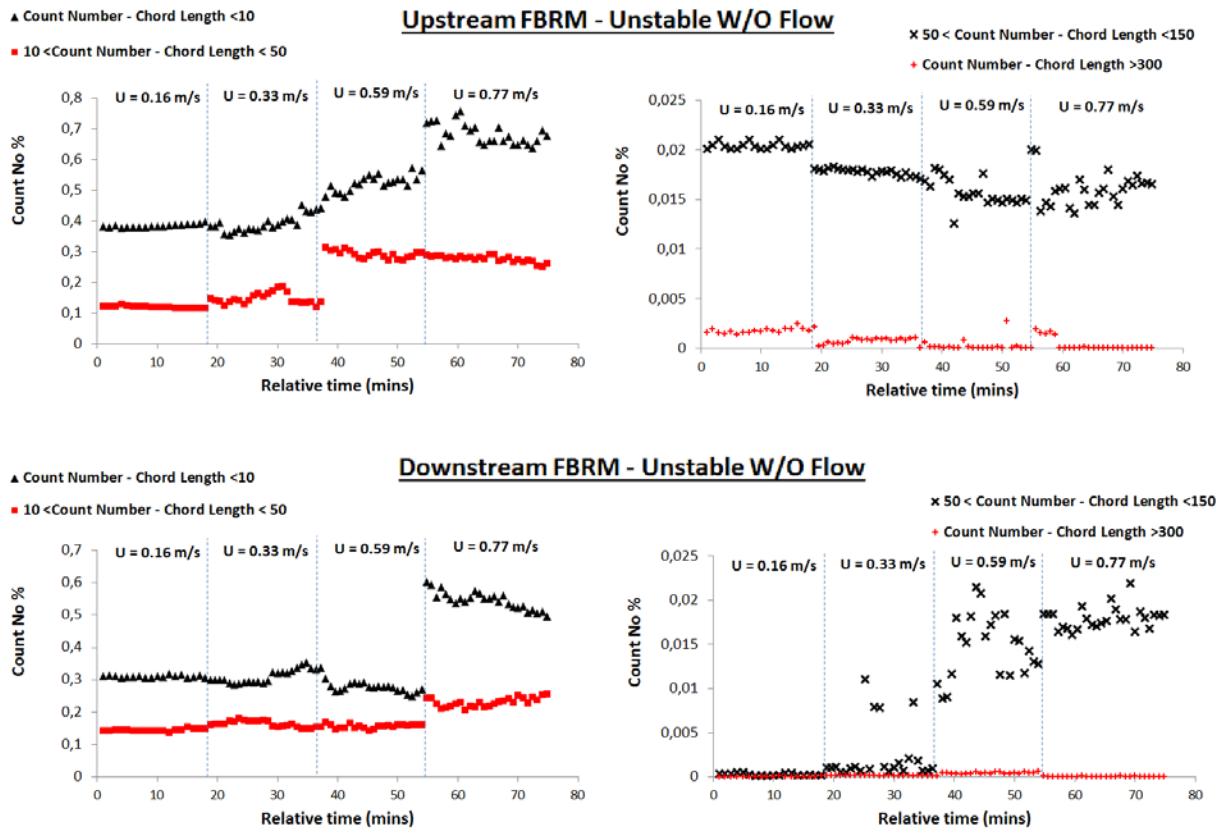
Figure 4.13: Effect of changes in velocity on chord length of droplets for the flow of unstable water-in-oil dispersion at water cut 10% in flow loop test.
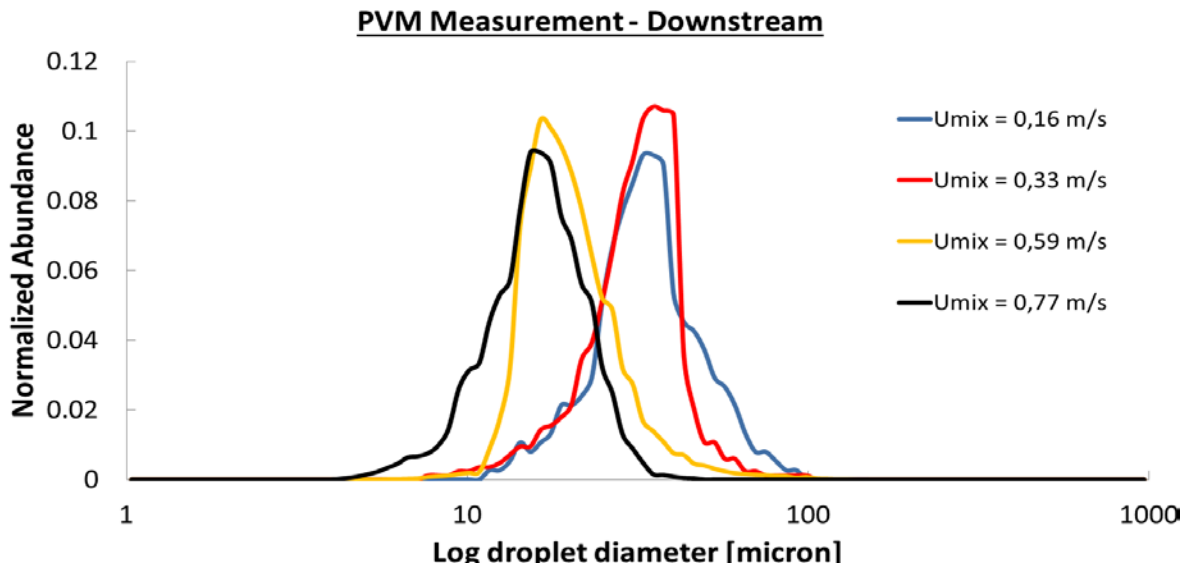

Figure 4.14: Effect of changes in velocity on DSD for the flow of unstable water-in-oil dispersion at water cut 10% in flow loop test.

42

4.2.2 Flow of stabilized water-in-oil dispersion

To stabilize the water dispersion, the surfactant was added to the flow in two steps, 0.05 wt% and 0.1 wt% of surfactant. The mixture velocity was changed from 0.18 m/s to 0.47 m/s for each case. Due to limitation in capturing PVM images(unclear rims of very small droplets), the test stopped at 0.47m/s. Figure 4.15 shows the count number of chord length in upstream and downstream for water-in-oil flow when 0.05wt% surfactant was added. At U=0.47 m/s, the number of chord length less than 50 microns in upstream is larger than downstream; However, the flow was not fully developed and needed more surfactant to be added. In addition, the figure 4.16 shows the dynamic change of DSD captured by PVM probes with increase in velocity of the flow.
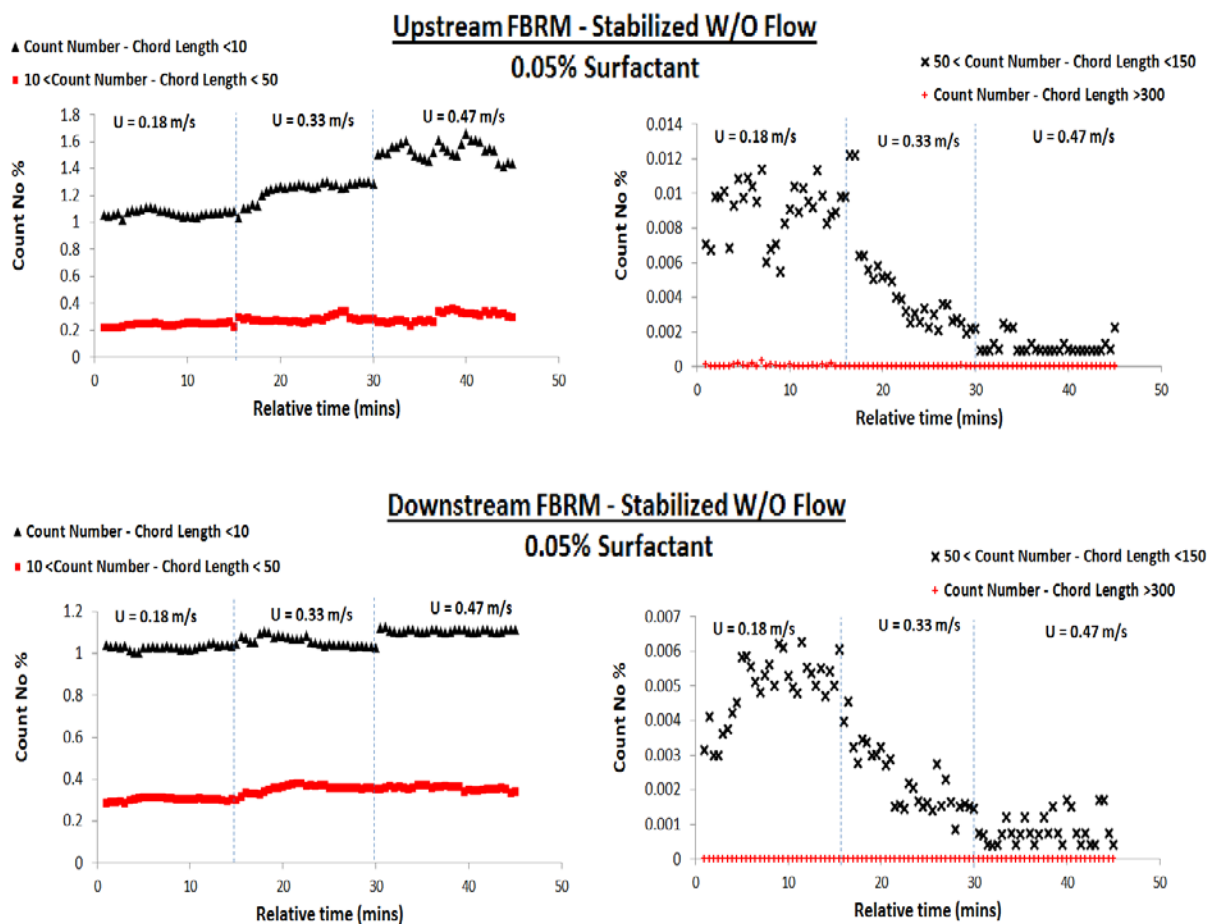

Figure 4.15: Effect of changes in velocity on chord length of droplets for the flow of stabilized water-in-oil dispersion at water cut 10% with 0,05 wt% surfactant added in flow loop test.

Figure 4.16: Effect of changes in velocity on DSD for the flow of stabilized water-in-oil dispersion at water cut 10% with 0,05wt % surfactant added in flow loop test.

Figure 4.17 shows the count number of chord length in upstream and downstream for water-in-oil flow when 0.1 wt% surfactant is added. The chord lengths divide into four groups. The numbers of chord length at upstream and downstream are almost the same. This means the flow was fully developed at velocity of 0.47 m/s in upstream and it continued to downstream. This is also clear in figure 4.19 that show the CLD profiles of the upstream and downstream FBRM together. The reduction in effect of distance between PVM probe and FBRM probes gives the possibility to compare the CLD and DSD. The CLD measured by downstream FBRM at U=0.47 m/s is chosen for the conversion to DSD and shown in figure 4.20.
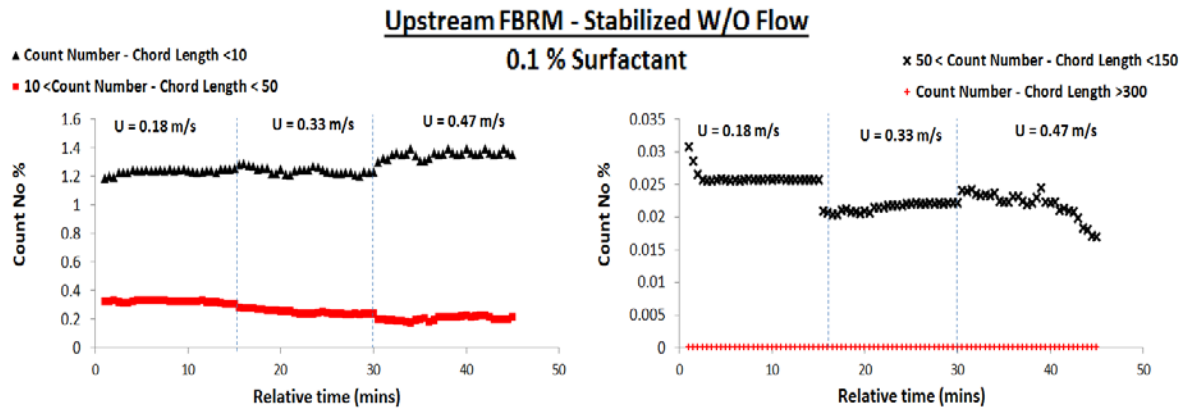
Figure 4.17: Effect of changes in velocity on chord length of droplets for the flow of stabilized water-in-oil dispersion at water cut 10% with 0.1 wt% surfactant added in flow loop test.
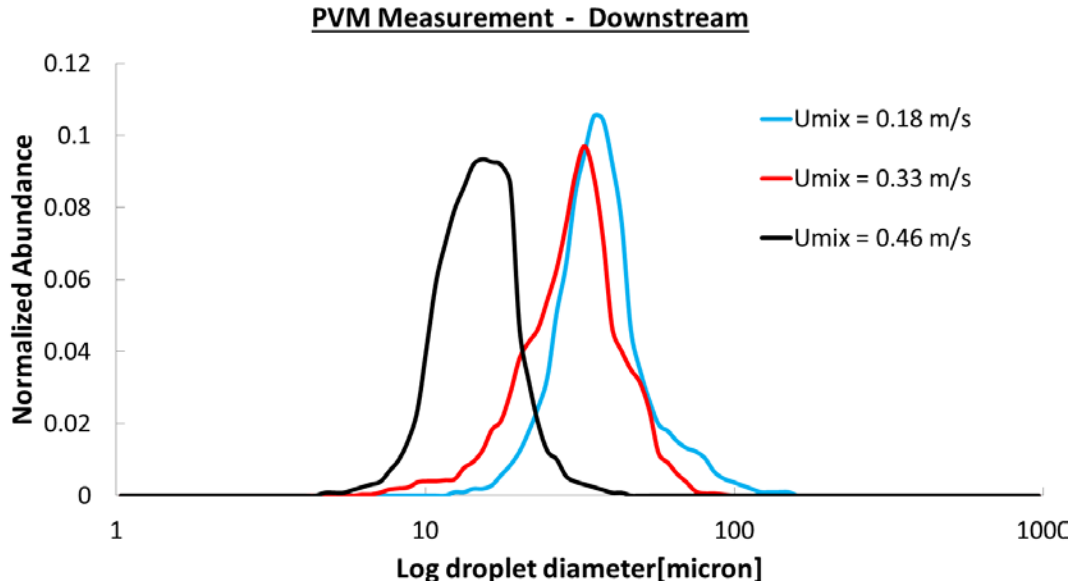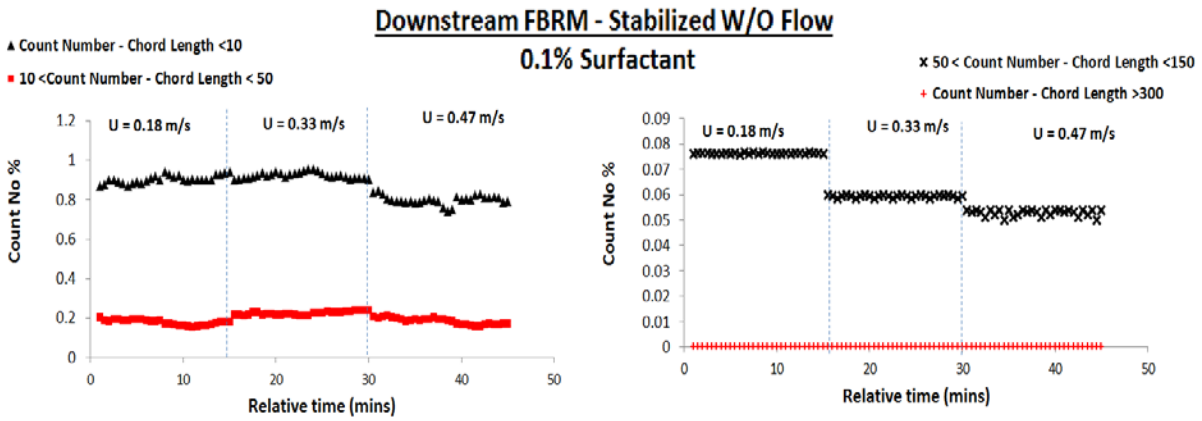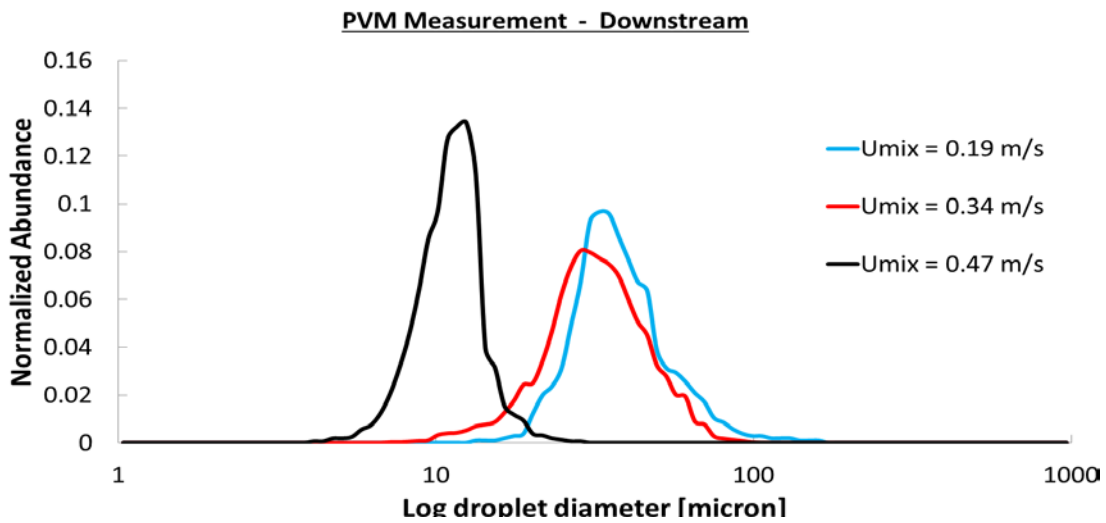

Figure 4.18: Effect of change in velocity on DSD for the flow of stabilized water-in-oil dispersion at water cut 10% with 0.1wt % surfactant added in flow loop test.
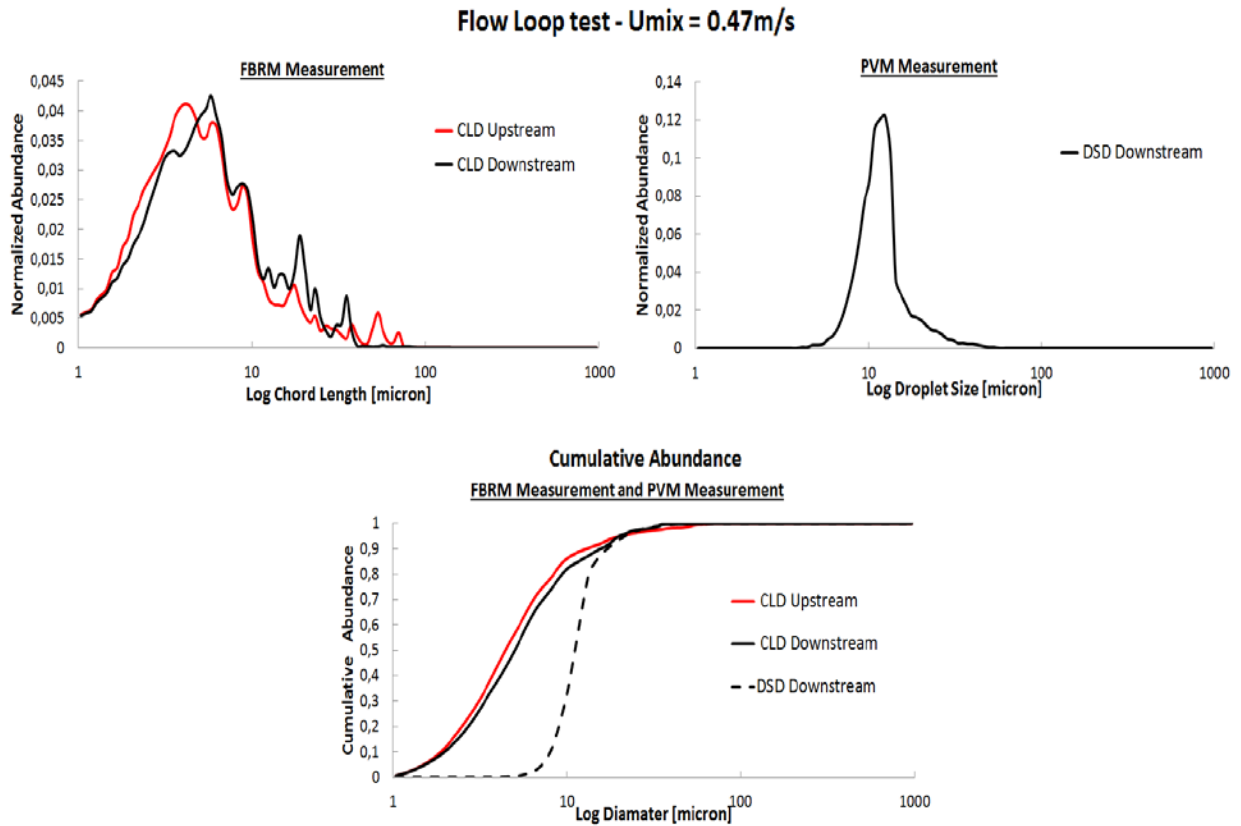
Figure 4.19: Normalized CLD in left picture, normalized DSD in right picture and both cumulative CLD and DSD in bottom picture.
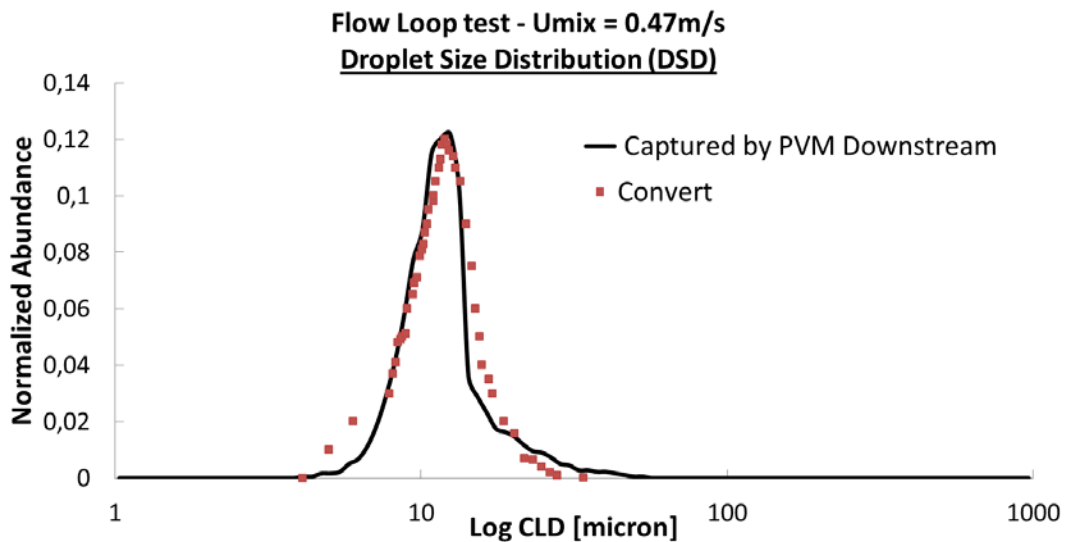
Figure 4.20: The experiment DSD measured by PVM probe and converted DSD for the flow of stabilized of water-in-oil dispersion at velocity U=0.47 m/s.

In this project two kinds of test were done, beaker test and flow loop test. According to the following reasons, The Beaker test is a good approximation on studying the uncertainty of FBRM probe in measuring the droplet size of the water-oil flow instead of using the close flow loop.

- The simplicity in running the beaker test and in controlling the temperature and rotational speed.
- The effect of distance between FBRM probes and PVM in the flow loop test. The flow should be completely developed in upstream and continued to downstream to have less effect of distance. So it causes to make the experiments with the flow loop very difficult.
- The results of water-in-oil flow in the flow loop test confirmed the CLD-DSD conversion model that was developed in beaker test.

5 Conclusion and Future Work

5.1 Conclusion

The experimental data in the present case studies provided a basis of comparison between the CLD measured by a FBRM probe and the DSD measured by a PVM probe. The droplet size was shown to be dramatically undersized by the FBRM probe for both the flow of water-in-oil dispersion and the flow of oil-in-water dispersion. An empirical fit was found to give reasonable agreement between the FBRM and PVM mean and maximum sizes measured for droplets. In this work, an experimental analysis gives us significant results:

- The PVM probe was found to be a useful tool for determining the droplet size distribution for different crude oils with a wide variety of viscosities.
- The exterior smooth surface of droplets was leading to strong errors in the measurement of the size of the droplets using FBRM probe. The FBRM probe undersized the droplet diameters of oil-water emulsions and water-oil emulsions by a factor of 43% - 56% for maximum droplet size.
- In stabilized water-in-oil dispersion, it was found that the PVM probe is limited to capturing the droplets larger than 5 μm.
- A universal conversion model was developed between the CLD and DSD based on experimental data and a log-normal distribution. This model is applicable to any oil-water system with various types of oil, different water cut, and different fluid properties including density, viscosity and surface tension.
- The mean droplet size was slightly overestimated with the PVM when the smallest droplets were not included, but this does not fully account for the under sizing of the droplets that was found using the FBRM probe.

Nevertheless, the chord length measured with the FBRM probe gives a good approximation of the droplet size distributions if the correction factors are considered. Due to using a good conversion CLD-DSD model, FBRM can be used for both the comparison and development of flow behavior models including maximum droplet size model and friction factor model.

5.2   Recommendations

- In the flow loop system, the current experiment was conducted using limited range of mixture velocity due to limitation in pressure transducer and limitation in capturing clear images using PVM probe. It would be interesting to study at higher velocity.
- In this project, only the flow of water-in-oil dispersion was employed in flow loop test. It would be better if some experiments would be done on the flow of oil-in-water dispersion and compared with the beaker test.
- In the experiment with flow loop test, only Exxsol oil was used. It would be interesting if other oils (i.e. Troll B and Grane) would be tested in flow loop.

6   References:

Angeli, P. and G. Hewitt (2000). "Flow structure in horizontal oil–water flow." International journal of multiphase flow **26**(7): 1117-1140.

Arirachakaran, S., K. Oglesby, et al. (1989). An analysis of oil/water flow phenomena in horizontal pipes. SPE Production Operations Symposium.

Baier, F. O. (2001). "Mass Transfer Charectristics of a Novel Gas-Liquid Contactor, The Advanced Buss Lopp Reactor." (Ph.D Dissertation, Swiss Federal Institute of Technology Zurich Switzerland).

Boxall, J. A., C. A. Koh, et al. (2009). "Measurement and calibration of droplet size distributions in water-in-oil emulsions by particle video microscope and a focused beam reflectance method." Industrial & Engineering Chemistry Research **49**(3): 1412-1418.

Greaves, D., J. Boxall, et al. (2008). "Measuring the particle size of a known distribution using the focused beam reflectance measurement technique." Chemical Engineering Science **63**(22): 5410-5419.

Group, M. T. L. P. (2004). "FBRM Control Interface version 6.0 Users Manual."

Heath, A. R., P. D. Fawell, et al. (2002). "Estimating average particle size by focused beam reflectance measurement (FBRM)." Particle & Particle Systems Characterization **19**(2): 84-95.

Hu, B., P. Angeli, et al. (2005). "Evaluation of drop size distribution from chord length measurements." AIChE journal **52**(3): 931-939.

Khatibi, M. (2012). "Study of droplet size distribution of viscous oil water flow." (Specialization project, Norwegian University of Science and Technology,NTNU and Statoil multiphase flow laboratory in Research, development and Innovation (RDI) in Rotvoll-Trodnheim).

Li, M., D. Wilkinson, et al. (2006). "Obtaining particle size distribution from chord length measurements." Particle & Particle Systems Characterization **23**(2): 170-174.

Lovick, J. and P. Angeli (2004). "Experimental studies on the dual continuous flow pattern in oil–water flows." International journal of multiphase flow **30**(2): 139-157.

O'SULLIVAN, B., B. SMITH, et al. (2010). "Optimization of particulate and droplet processes using FBRM® and PVM® technologies." Inżynieria i Aparatura Chemiczna Selected full texts(4): 76-77.

Packer, K. and C. Rees (1972). "Pulsed NMR studies of restricted diffusion. I. Droplet size distributions in emulsions." Journal of Colloid and interface Science **40**(2): 206-218.

Rizon, M., Y. Haniza, et al. (2005). "Object detection using circular Hough transform." American Journal of Applied Sciences **2**(12): 1606-1609.

Ruf, A., J. Worlitschek, et al. (2001). "Modeling and experimental analysis of PSD measurements through FBRM." Particle & Particle Systems Characterization **17**(4): 167-179.

Turner, D. (2005). "Clathrate hydrate formation in water-in-oil dispersions." (Ph.D. Dissertation, Colorado School of Mines, Golden, CO).

7 Attachments

7.1 Attachment I: Matlab Codes of Post Processing of PVM Images

For running the Matlab codes to detect the droplets circle and make the droplets distribution, it is needed to have the license of image processing toolbox in Matlab. The codes for this purpose are shown as below:

% % Detection of droplets

```
radiust1=zeros(25,100);
radiust2=zeros(25,100);
radiust3=zeros(25,100);
radiust4=zeros(25,100);
radiust5=zeros(25,100);
D=(Rizon, Haniza et al. 2005);
for i=1:100
K=i-1;
D(Baier)=strcat(num2str(K),'.bmp');
I = imread(D(Baier));
figure, imshow(I), title('original image');
```

%%Image Binarisation (Adjustment)

```
background = imopen(I,strel('disk',100));
I2 = I - background;
figure, imshow(I2)
```

%%Morphological Opening on Grayscale, and Dilating images

```
I3 = imadjust(I2);
figure, imshow(I3);
level = graythresh(I2);
bw = im2bw(I3,level);
bw = bwareaopen(bw, 100);
figure, imshow(bw);
[junk threshold] = edge(bw, 'prewitt');
fudgeFactor = 0.1;
BWs = edge(I,'prewitt', threshold * fudgeFactor);
figure, imshow(BWs), title('binary gradient mask');
se90 = strel('line', 4, 90);
se0 = strel('line', 4, 0);
BWsdil = imdilate(BWs, [se90 se0]);
figure, imshow(BWsdil), title('dilated gradient mask');
```

%% measuring the diameter

```
imshow(I)
[center1, radius1] = imfindcircles(BWsdil,[10 , 50], 'Sensitivity',0.60, 'EdgeThreshold', 0.3,
'ObjectPolarity', 'bright', 'Method', 'TwoStage')
);
[center2, radius2] = imfindcircles(BWsdil,[51 , 100], 'Sensitivity',0.60, 'EdgeThreshold', 0.3,
'ObjectPolarity', 'bright', 'Method', 'TwoStage');
[center3, radius3] = imfindcircles(BWsdil,[101 , 200], 'Sensitivity',0.60, 'EdgeThreshold',
0.3, 'ObjectPolarity', 'bright', 'Method', 'TwoStage');
[center4, radius4] = imfindcircles(BWsdil,[201 , 300], 'Sensitivity',0.60, 'EdgeThreshold',
0.3, 'ObjectPolarity', 'bright', 'Method', 'TwoStage');
```

```
[center5, radius5] = imfindcircles(BWsdil,[301 , 600], 'Sensitivity',0.60, 'EdgeThreshold',
0.3, 'ObjectPolarity', 'bright', 'Method', 'TwoStage');
```

%%Display the circle

```
 imshow(BWsdil)
viscircles(center1,radius1);
viscircles(center2,radius2);
viscircles(center3,radius3);
```

%%Adding diameters into the separate charts

```
radiust1(1:numel(radius1),i)=radius1(:,1);
if size(radius2)~=[0,0];
radiust2(1:numel(radius2),i)=radius2(:,1);
end
if size(radius3)~=[0,0];
radiust3(1:numel(radius3),i)=radius3(:,1);
end
if size(radius4)~=[0,0];
radiust4(1:numel(radius4),i)=radius4(:,1);
end
if size(radius5)~=[0,0];
radiust5(1:numel(radius5),i)=radius5(:,1);
end
end
```

%%Processing the charts for different range of diameter

```
 radt=[];
for j=1:100
   r1=radiust1(:,j);   r1(r1==0)=[];   r2=radiust2(:,j);   r2(r2==0)=[];   r3=radiust3(:,j);   r3(r3==0)=[];
   r4=radiust4(:,j);   r4(r4==0)=[];   r5=radiust5(:,j);   r5(r5==0)=[];   radt(1:numel(r1),j)=r1(:,1);

if size(r2)~=[0,0];
   radt(numel(r1)+1:numel(r1)+numel(r2),j)=r2(:,1);
end
if size(r3)~=[0,0];
    radt(numel(r1)+numel(r2)+1:numel(r1)+numel(r2)+numel(r3),j)=r3(:,1);
end
if size(r4)~=[0,0];
    radt(numel(r1)+numel(r2)+numel(r3)+1:numel(r1)+numel(r2)+numel(r3)+numel(r4),j)=r4(:,1);
end
if size(r5)~=[0,0];

radt(numel(r1)+numel(r2)+numel(r3)+numel(r4)+1:numel(r1)+numel(r2)+numel(r3)+numel(r4)+numel(r5),j)=r5(:,1
);
end
end

diameter=radt*2*1.5;
```

7.2 Attachment II: Tables and Figures Results (Beaker and Flow Loop test)

The relevant tables and figures are represented here. The excel sheets of the data and process analysis has been attached to the report.

Beaker Test:

Table II.1: Parametric measurement with FBRM and PVM for Exxsol oil - water flow (WC=10%-90%)

WC	Speed	d_{32}	d_{43}	$d_{99\text{-volume}}$	d_{32}	d_{43}	$d_{99\text{-volume}}$
%	RPM	FBRM	FBRM	FBRM	PVM	PVM	PVM
10	1500	56	82	400	192	203	353
30	1500	63	70	227	213	222	401
70	1500	68	73	235	225	237	411
90	1500	59	43	189	184	193	346

Table II.2: Parametric measurement with FBRM and PVM for Troll B oil water flow (WC=10%-90%)

WC	Speed	d_{32}	d_{43}	$d_{99\text{-volume}}$	d_{32}	d_{43}	$d_{99\text{-volume}}$
%	RPM	FBRM	FBRM	FBRM	PVM	PVM	PVM
10	1500	37	76	872	118	128	266
30	1500	33	68	151	103	118	320
70	1500	36	83	202	128	160	394
90	1500	53	90	254	135	158	359

Table II.3: Parametric measurement with FBRM and PVM for Grane oil water flow (WC=10%-90%)

WC	Speed	d_{32}	d_{43}	$d_{99-volume}$	d_{32}	d_{43}	$d_{99-volume}$
%	RPM	FBRM	FBRM	FBRM	PVM	PVM	PVM
60	1500	146	239	865	221	235	421
70	1500	66	91	175	215	227	400
90	1500	40	38	305	293	368	802

Table II.4: Parametric measurement with FBRM and PVM for stabilized water-in-oil dispersion (Exxsol oil, WC=10%, and 0.1wt% surfactant is added)

Speed	d_{32}	d_{43}	$d_{99-volume}$	d_{32}	d_{43}	$d_{99-volume}$
RPM	FBRM	FBRM	FBRM	PVM	PVM	PVM
400	19	20	69	52	75	171
700	30	57	495	29	53	80
1000	41	70	550	20	28	69
1300	56	108	847	16	22	40
1500	76	152	888	8	10	28
1700	81	174	948	7	9	26
2000	87	187	902	6	8	21

Flow Loop Test:

Table II.5: Parametric measurement with pressure transducer (length 3m) for water-in-oil dispersion flow (Exxsol oil and WC=10%)

Umix	Temp	PDT1	PDT2
m/s	°c	mbar/m	mbar/m
0,16	22	5,8	34,4
0,33	22,3	8,7	118,5
0,47	22,7	14,8	206,6
0,59	23,3	19,1	306,2
0,70	24	23,0	425,6
0,77	25,6	25,1	498,5

Table II.6: Parametric measurement with pressure transducer (length 3m) for water-in-oil dispersion flow (Exxsol oil, WC=10%, and 0.05wt% surfactant is added)

Umix	Temp	PDT1	PDT2
m/s	°c	mbar/m	mbar/m
0,18	26,4	7,5	40,8
0,33	25,9	9,2	126,0
0,46	25,8	12,4	224,0

Table II.7: Parametric measurement with pressure transducer (length 3m) for water-in-oil dispersion flow (Exxsol oil, WC=10%, and 0.1wt% surfactant is added)

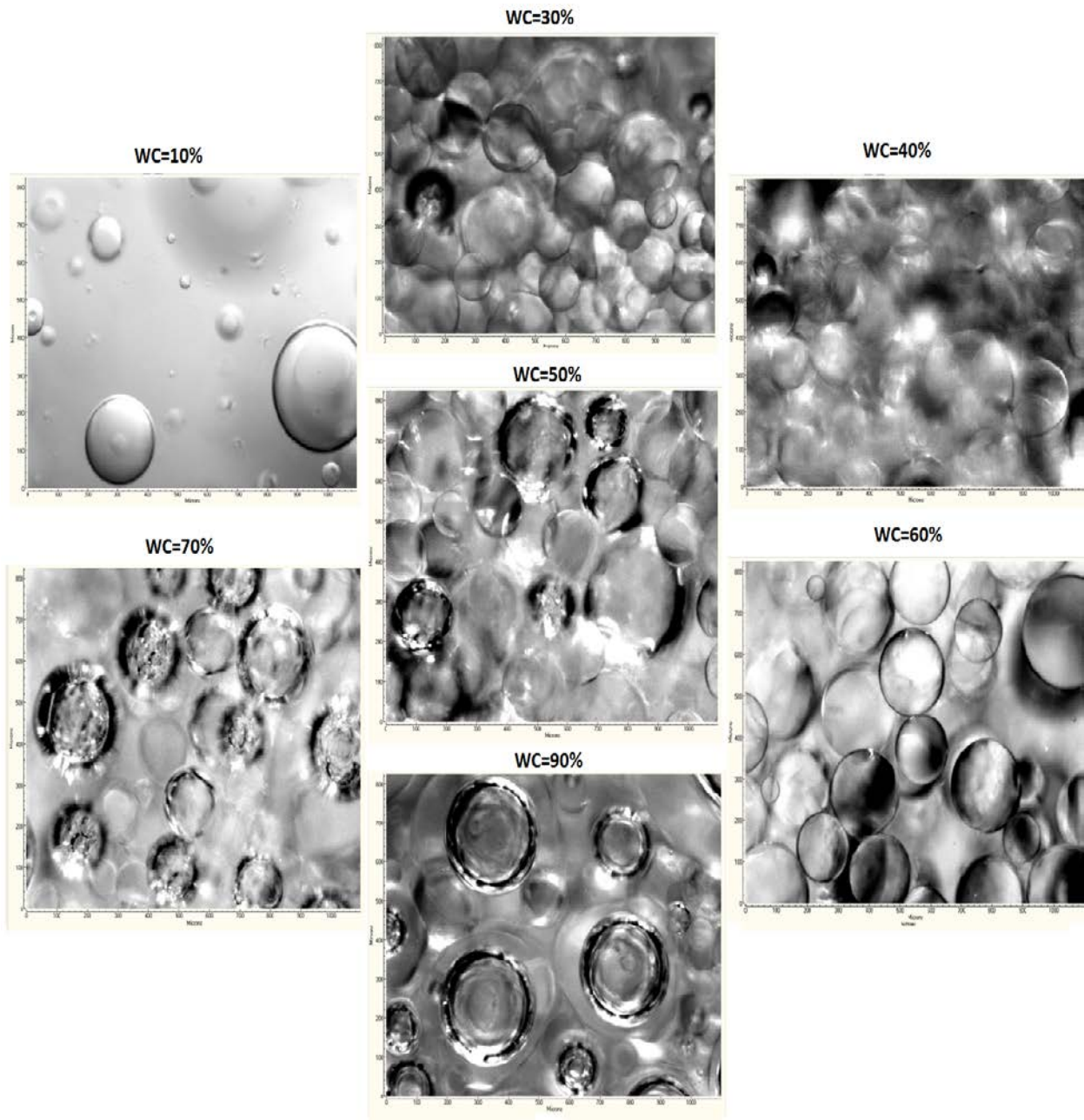| Umix	Temp	PDT1	PDT2
m/s	°c	mbar/m	mbar/m
0,19	24,6	6,8	49,8
0,34	23,4	9,3	128,2
0,47	23,4	13,1	226,1

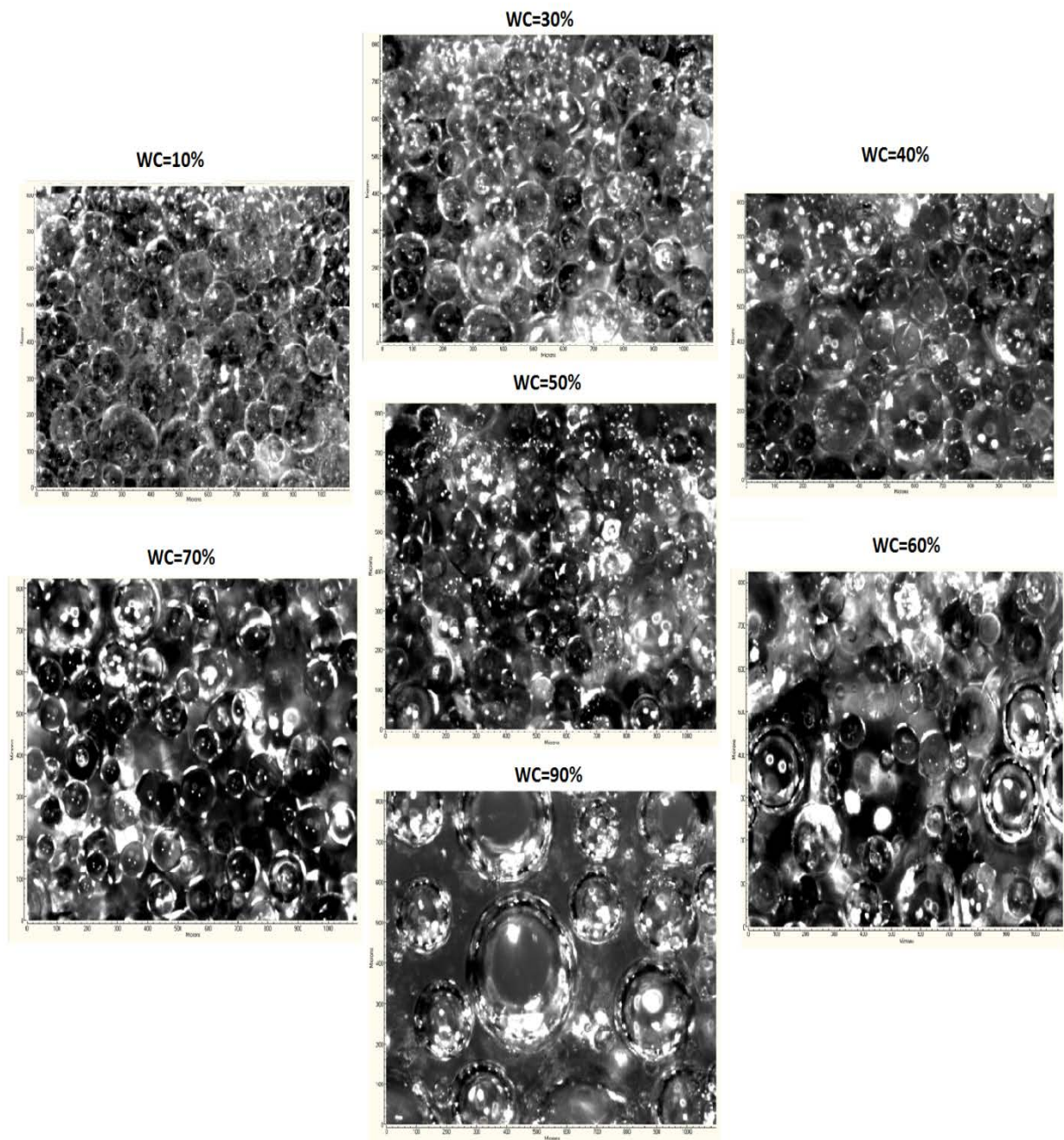Figure II.1: Exxsol oil at different water cut (10% - 90%)
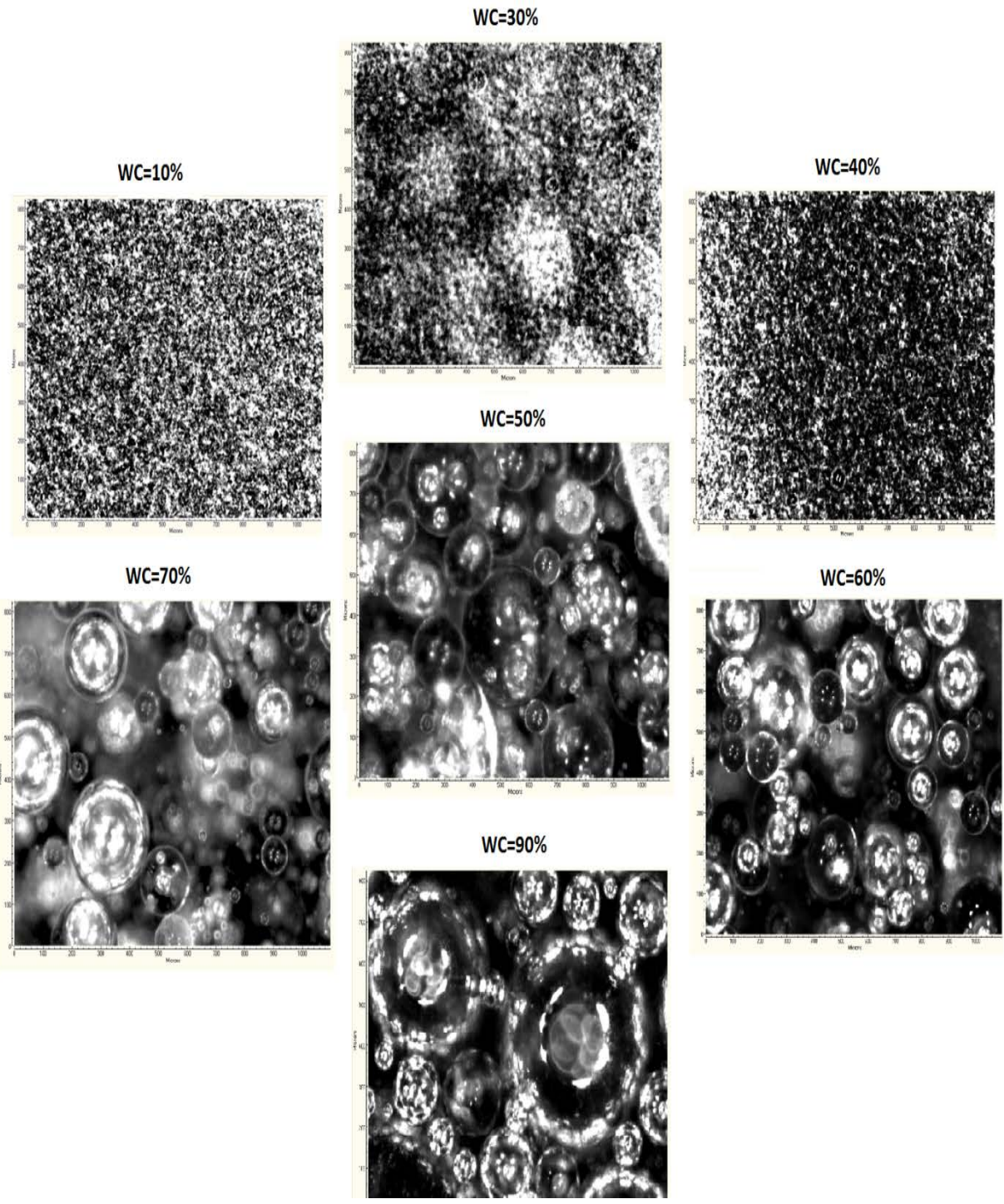
Figure II.2: Troll B oil at different water cut (10% - 90%)

Figure II.3: Grane oil at different water cut (10% - 90%)